Chinese Chemical Letters 33 (2022) 4478–4494

Contents lists available at ScienceDirect

Chinese Chemical Letters

journal homepage: www.elsevier.com/locate/cclet

Recent advance of fluorescent probes for detection of drug-induced liver injury markers

Dongqin Sun[a], Zhenzhen Chen[a], Jiali Hu[a], Huajin Zeng[a,*], Lingbo Qu[b], Ran Yang[b,*]

[a] School of Pharmaceutical Sciences, Zhengzhou University, Zhengzhou 450001, China
[b] The College of Chemistry, Zhengzhou University, Zhengzhou 450001, China

ARTICLE INFO

Article history:
Received 27 September 2021
Revised 22 November 2021
Accepted 18 December 2021
Available online 22 December 2021

Keywords:
Fluorescent probe
Drug-induced liver injury (DILI)
Roussel uclaf causality assessment method (RUCAM)
Clinical markers
Imaging

ABSTRACT

Drug-induced liver injury (DILI) is a common and serious adverse drug reaction. At present, DILI is perfectly diagnozed in clinical settings using Roussel Uclaf causality assessment method (RUCAM) in its original version published 1993 and its updated version published 2016, well established worldwide as a diagnostic algorithm with a high sensitivity and specificity. Nevertheless, the search for additional detection methods supporting RUCAM continues. In recent years, with the development of optical imaging technology, fluorescent probes have gradually shown great advantages in the detection and diagnosis of DILI markers such as high sensitivity, anti-interference, real-time monitoring and non-invasive measurement. In this review, the recent advances of fluorescent probes for evaluation of DILI in experimental studies were summarized according to various markers of DILI. We believe that learning about the design and practical application of these probes will contribute to the further development of detection sensors for DILI markers.

1. Introduction

Drug toxicity is not only a critical evaluation index of medicinal safety in the process of drug development, but also the main reason for drug withdrawal from the market. As one of the main metabolic organs, liver not only precisely coordinates with almost all organs in the body to maintain homeostasis, but also transforms drugs into various metabolites [1,2]. Therefore, when taking toxic drugs or overdose drugs, the liver is very vulnerable to drug injury. Drug-induced liver injury (DILI) refers to the liver injury caused by the drug itself and/or its metabolites in the course of medication. Nowadays, DILI is regarded as an important public health problem due to its unpredicatability and severity degree. In clinical practice, DILI is mainly judged according to the updated Roussel Uclaf causality assessment method (RUCAM) evaluation causality published in 2016, and the relationship between alanine aminotransferase (ALT), alkaline phosphatase (ALP) and their upper limit of normal (ULN) in serum is regarded as the gold standard marker for the diagnosis and evaluation of DILI [3–5]. However, these enzyme markers often can not reflect the abnormal state of DILI in real-time, because only a few patients showed abnormal enzyme level in early DILI. Moreover, rotavirus infection and skeletal muscle injury can also cause the increase of ALT [6,7]. Therefore, it is urgent to develop a method to monitor other markers directly related to DILI in real time.

Generally, the metabolism of drugs in the liver is divided into two stages: phase I reaction and phase II reaction [8]. In phase I, the main reactions are oxidation, reduction and hydrolysis, resulting in a serious of hepatotoxic products, such as electrophilic radicals and hydroxyl radicals. While, in phase II, binding reaction is the main metabolic process, which is a detoxification process of drugs [9,10]. If the process can not be carried out smoothly or untimely, it may cause liver injury. In order to explain the metabolism of drugs in liver more clearly, acetaminophen (APAP) can be used as a typical example of drug injury. As shown in Scheme 1, the overdose of APAP is *N*-hydroxylated first and then hydrolyzed by the CYP450 enzyme to form toxic *N*-acetyl-*p*-benzoquinone imine (NAPQI) [11,12]. Some NAPQI will combine with glutathione (GSH) to form nontoxic metabolies, while the remaining NAPQI will bind to the proteins in the body and release a large number of active substances, such as reactive nitrogen species (RNS), reactive oxygen species (ROS), reactive sulfur species (RSS), enzyme. These released active substances covalently bind to cellular proteins, which leads to cell peroxidation and apoptosis [13,14]. Meanwhile, various active substances may produce more active substances under the catalysis of enzymes, resulting in

* Corresponding authors.
E-mail addresses: zenghuajin@sina.com (H. Zeng), yangran@zzu.edu.cn (R. Yang).

https://doi.org/10.1016/j.cclet.2021.12.043
1001-8417/

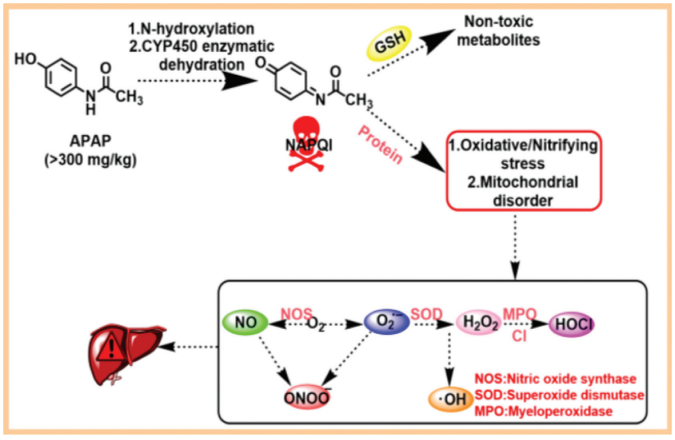

Scheme 1. The mechanism of liver injury induced by APAP and the associations between active substances.

serious liver injury. Therefore, compared with the levels of enzymes *in vivo*, these active substances can more accurately reflect DILI in real time, even in the early stage of DILI. Recently, with the development of optical imaging technology, more and more small molecule probes have been designed for detection of these active substances, including peroxynitrite ($ONOO^-$), nitric oxide (NO), superoxide anion ($O_2^{\bullet-}$), hypochlorous acid (HClO), hydrogen peroxide (H_2O_2), hydroxyl radical ($^{\bullet}OH$), GSH, hydrogen sulfide (H_2S) and enzymes.

To better design novel probes for diagnosis of DILI, different types of probes were summarized according to the various markers of DILI. We believe that these reported probes will promote the further development of DILI detection sensors.

2. Small molecule probes for detecting various DILI markers

2.1. Detection of $ONOO^-$

As a member of RNS, peroxynitrite ($ONOO^-$) possesses a strong ability of oxidation and nitrification and is produced by the reaction of nitric oxide (NO) with superoxide anion ($O_2^{\bullet-}$) *in vivo*. It is reported that excessive $ONOO^-$ will react with various biological molecules and cause the destruction of cell structure and function, even apoptosis and necrosis [15,16]. Compared to other ROS and RNS, $ONOO^-$ is more attractive and regarded as a direct marker of DILI. Recently, a lot of small molecule probes have been developed for detection of $ONOO^-$ *in vitro* and *in vivo* based on different reaction mechanisms.

(1) Decomposition of α-keto amide group. Previous studies have shown that under physiological conditions the α-keto esters can react with $ONOO^-$ [17] (Scheme 2A). According to this reaction mechanism, Yang's team proposed that deprotection of the α-keto caged fluorophore might produce a particular "turn-on" probe for $ONOO^-$ [16], and the detailed reaction mechanism was shown in Scheme 2B. The amino group on the fluorophore was protected by phenylglyoxylic acid on the α-keto caged structure, thereby inhibiting the intramolecular charge transfer (ICT) and promoting photo-induced electron transfer (PET) effects which made the fluorescence quenching. When the probes reacted with $ONOO^-$, the α-keto site was first subjected to nucleophilic attack and released NO_2 and generated highly reactive epoxide. After that, an anhydride was yielded by intramolecular rearrangement. Finally, the anhydride hydrolyzed to dissociate into amino groups and carboxylic acid which made the fluorescence status of probes change from "turn-off" to "turn-on".

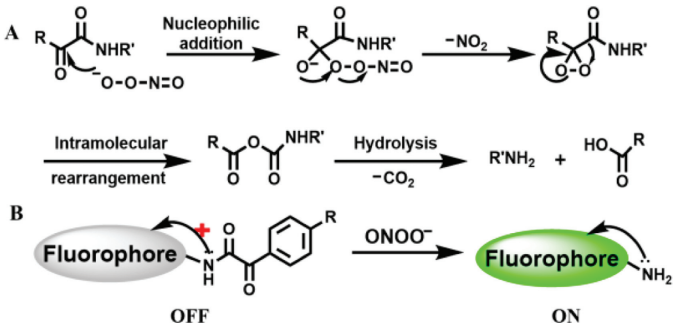

Scheme 2. Proposed reaction mechanism of $ONOO^-$ with α-keto esters (A) and α-keto caged fluorophore (B).

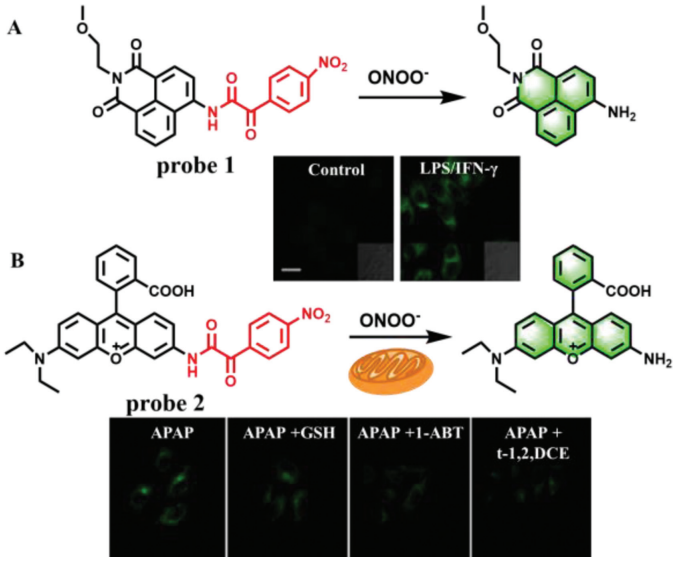

Fig. 1. (A) The reaction mechanism of probe **1** for $ONOO^-$ and fluorescence imaging in HepG2 cells. (B) The reaction mechanism of probe **2** for $ONOO^-$ and the fluorescence imaging of APAP-induced hepatotoxicity and remediation in HepG2 cells. Copied with permission [18]. Copyright 2017, American Chemical Society.

To test this proposal, Cheng *et al.* designed two fluorescence probes by linking an α-keto amide to aminonaphthalimide (Naph-$ONOO^-$ probe, probe **1**) (Fig. 1A) and rhodamine (Rhod-$ONOO^-$ probe, probe **2**) (Fig. 1B), respectively [18]. Both of probes could specifically and sensitively detect $ONOO^-$ in living cells in real time. More importantly, probe **2** could accumulate and react in mitochondria with a substantial high sensitivity of 43 nmol/L. Subsequently, several fluorescence probes with similar α-keto caged structures were developed, such as probes **3**–**6** (Fig. 2) [18–22]. Details of these probes were summarized in Table 1.

(2) Transformation of phenylborate to phenol. Compared with the visible and the first near-infrared regions (NIR-I), recently the second near-infrared regions (NIR-II, 900–1700 nm) has been attracted great attention because of its deep penetration into biological tissues (5–20 mm), the reduction of background auto-fluorescence and the improvement of signal-to-noise ratio (SNR) [23]. In 2019, Li group designed an NIR-II fluorescence probe (IRBTP, probe **7**), which combined the phenyl borate group and benzothiopyrylium cyanines skeleton for monitoring of $ONOO^-$ [24]. When $ONOO^-$ is present, the phenyl borate group was removed and fluorescence at 950 nm will appear (Fig. 3A), which the fluorescence intensity enhanced with the increase of $ONOO^-$ concentrations ranged from 0 μmol/L to

Table 1
Fluorescence probes for detection of $ONOO^-$ based on decomposition of α-keto amide group.

Probe	$\lambda_{ex}/\lambda_{em}$ (nm)	Linear range	Equation (*R*-square)	LOD	Analytical samples	Year	Ref.
1	450/546	0–25 μmol/L	$y = 610.5806x + 283.5541$ ($R^2 = 0.9961$)	79 nmol/L	Living cells	2017	[18]
2	500/558	0–16 μmol/L	$y = 2620.6912x + 51.0045$ ($R^2 = 0.9956$)	43 nmol/L	Living cells	2017	[18]
3	430/560	0–10 μmol/L	$y = 11{,}698.0600x + 9086.5000$ ($R^2 = 0.9950$)	25 nmol/L	Living cells, mice	2017	[19]
4	345/600	0.5–10 μmol/L	–	200 nmol/L	Living cells, mice	2018	[20]
5	660/706	0–15 μmol/L	$y = 112.0940x + 78.8250$ ($R^2 = 0.9940$)	90 nmol/L	Living cells, mice	2019	[21]
6	410/560	0–9 μmol/L	$y = 32{,}514.1334x + 43{,}863.1116$ ($R^2 = 0.9967$)	31 nmol/L	living cells, tissues	2020	[22]

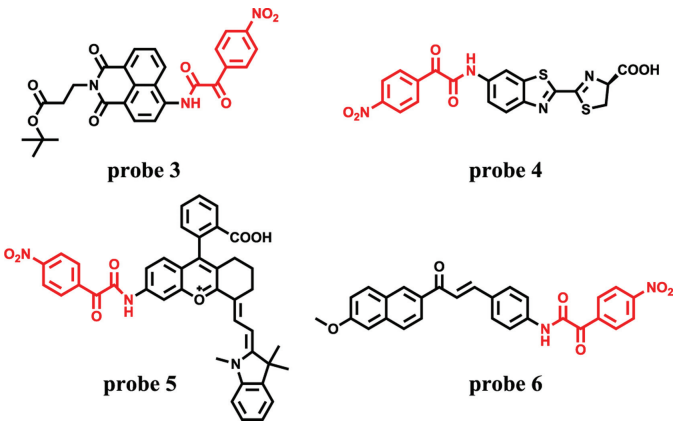

Fig. 2. The structures of probes **3**–**6**.

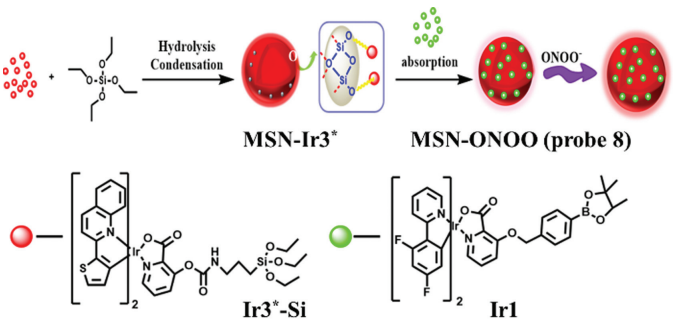

Fig. 4. The reaction mechanism of probe **8** with $ONOO^-$.

11 μmol/L (LOD = 55.9 nmol/L). Tissue imaging demonstrated that the liver of mouse appeared obvious fluorescence after APAP treatment, even the penetration depth reached 5 mm (Figs. 3B and C), which laid a foundation for effectively detecting the fluctuation of $ONOO^-$ in preclinical model of DILI.

Recently, due to its good photostability and high luminescent quantum efficiency, phosphorescent transition metal complex has attracted researchers' interest in bioluminescence probes. In 2018, Chen *et al.* developed a dual-emission phosphorescent peroxynitrite nanoprobe (MSN–ONOO, probe **8**, Fig. 4) by modifying two long-lived phosphorescent iridium(III) complexes (Ir1 and Ir3*) with peroxynitrite activity and inertness into mesoporous silica nanoparticles (MSN) [25]. Due to fast response and high sensitivity, as well as good selectivity, probe **8** was used to the determination of $ONOO^-$ in living cells, zebrafishes and mice *via* ratiometric photoluminescence imaging. What is more important, by virtue of long-lived phosphorescence, probe **8** imaged the elevated $ONOO^-$ during DILI *in vivo* while reducing spontaneous fluorescence and improving SNR.

(3) Oxidation of phenol. The results of probe **7** and **8** suggested that it is an efficient strategy to develop fluorescence probe by masking hydroxyl functionalized reaction sites with a trigger of $ONOO^-$. In order to further improve the targeting of the probe, Zhou's team constructed a peroxisome-targeting two-photon (TP) fluorescence probe (PX-1, probe **9**) for detection of peroxisomal $ONOO^-$ [26]. In the structure of probe **9**, the 1,8-naphthalene was served as fluorophore, while the nonapeptide (HLKPLQSKL) was regarded as a peroxisome-targeting group. After reacting with $ONOO^-$, the 1,4-dihydroxybenzene of probe **9** was removed, resulting in a 300-fold fluorescence enhancement

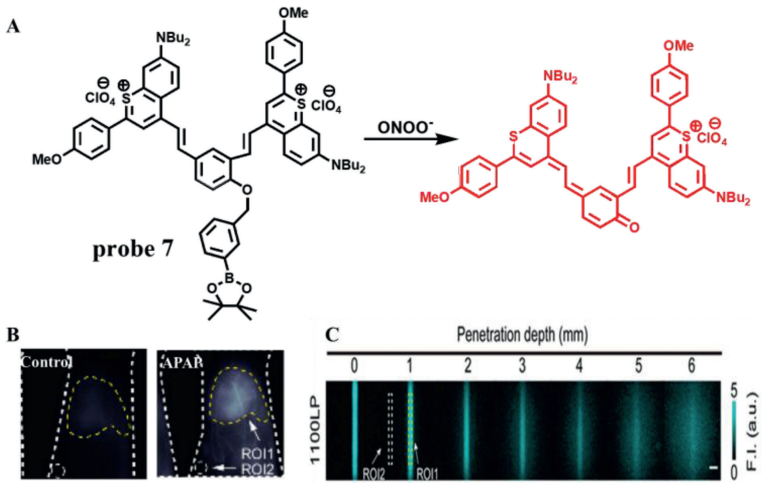

Fig. 3. (A) The reaction mechanism of probe **7** with $ONOO^-$. (B) The imaging of mouse liver treated with APAP. ROI1–Signal intensity of liver area. ROI2–Background signal intensity. (C) The penetration depth of fluorescence imaging. ROI1–Average signal intensity. ROI2–Average background signal intensity. The SNR is obtained by dividing ROI by ROI2. Copied with permission [24]. Copyright 2019, American Chemical Society.

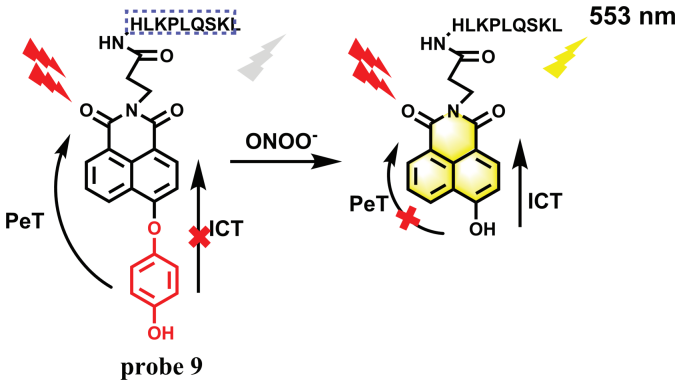

Fig. 5. The sensing mechanism of probe **9** with ONOO⁻.

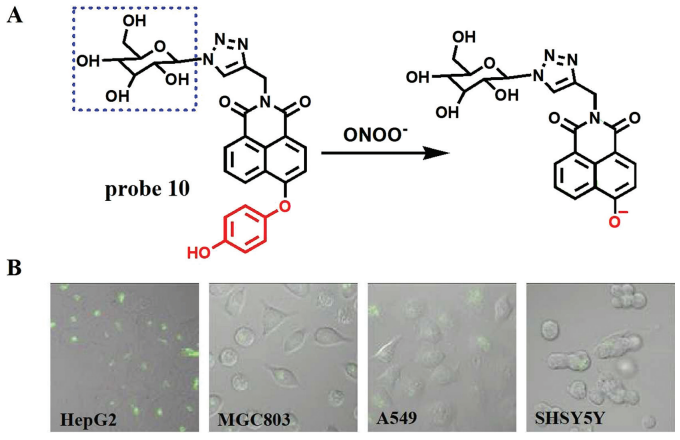

Fig. 6. (A) The reaction mechanism of probe **10** with ONOO⁻. (B) The fluorescence imaging of different cells incubated with probe **10**. Copied with permission [29]. Copyright 2019, Elsevier.

(LOD = 6.2 nmol/L) at 553 nm (Fig. 5). The imaging results demonstrated that probe **9** could significantly detect and map ONOO⁻ in SMMC-7721 cells when they pre-treated with sydnonumine hydrochloride (SIN-1, an ONOO⁻ donor). However, when these stimulated cells were incubated with uric acid (an ONOO⁻ scavenger), their red fluorescence was remarkably inhibited, demonstrating that probe **9** can sensitively identify the fluctuations of ONOO⁻ in living cells. The results were further confirmed in the livers of CCl_4-treated mice. However, due to the limitation of targeting, the incubation time of 30 min may not be suitable for real-time monitoring of DILI.

Several studies have shown that the asialoglycoprotein receptor on hepatoma cells can specifically recognize galactose [27,28]. According to this characteristic, Liu team designed and synthesized a galactose-based hepatoma-specific fluorescence probe (Gal-NHP, probe **10**) for imaging endogenous ONOO⁻ in HepG2 cells [29]. As expected, due to the ICT effect, the fluorescence of fluorophore 4–hydroxy-1,8-naphthlimide on probe **10** was suppressed by 1,4-dihydroxybenzene. However, after reacting with ONOO⁻, a remarkable emission peak at 555 nm was observed and a good linear relationship between the fluorescence intensity and ONOO⁻ concentrations was obtained with a LOD of 20 nmol/L (Fig. 6A). The imaging results from four kinds of living cells including HepG2, MGC803, A549 and SHSY5Y showed that the probe exhibited excellent specificity towards ONOO⁻ in HepG2 cells over others (Fig. 6B), which confirmed that probe **10** could specifically target hepatoma cells and use in the study of ONOO⁻-related liver diseases.

More recently, Jin's team designed a novel fluorescent probe (probe **11**) for detection of ONOO⁻ during acute liver injury through a phenol oxidation mechanism similar to the probe **10** [30]. The probe is essentially non-fluorescent, however, after rapid reaction with ONOO⁻ (< 25 s), the phenol structure falls off and forms conjugation, showing obvious fluorescence at 560 nm (Fig. 7A). With the increase of ONOO⁻ concentration from 0 μmol/L to 10 μmol/L, a linear relationship was obtained between fluorescence intensity and concentrations and the LOD is detected to be 0.13 μmol/L without any interference by other substances. In addition, When LX-2 cells were stimulated by SIN-1, LPS and PMA, the fluorescence increased, while the fluorescence decreased after N-acetylcysteine (NAC) and FeTMPyP pretreatment, which proved that probe **11** could not only detect endogenous and exogenous ONOO⁻, but also monitor the remediation of DILI (Fig. 7B). Most importantly, when APAP induced acute liver injury in mice (Fig. 7C), the fluorescence of mouse liver region was significantly enhanced, which was consistent with the results at the cell level. At the same time, immunohistochemistry and imaging examination further verified the degree of drug-induced liver injury, which laid a solid foundation for the probe to monitor ONOO⁻ in the process of DILI.

(4) Breakage of unsaturated double bond. Generally, ONOO⁻ and HClO can break the unsaturated double bond simultaneously. Due to many excellent characteristics, such as high photostability and high SNR, nanoparticles have been applied in many fields, including nanoprobe. In 2017, Peng *et al.* developed a multilayered lanthanide-doped upconversion nanoparticles (UCNPs) modified with polyethylenimine and a fluorophore cyanine (Cy7) as a nanoprobe (Cy7-PEI-UCNPs, probe **12**) for detection of ONOO⁻ (Fig. 8A) [31]. As expected, with the increase of ONOO⁻ concentrations from 3.5 μmol/L to 17.5 μmol/L, the fluorescence intensity of probe **12** was enhanced gradually, which resulted from the breaking of the double bond of Cy7. Moreover, probe **12** offered a low LOD down to 0.08 μmol/L and a fast response toward ONOO⁻ less than 1 s. Imaging results of APAP-induced mice demonstrated that probe **12** was primarily concentrated in the liver, which was suitable for monitoring ONOO⁻ generated in the model of acute hepatotoxicity (Fig. 8B). Subsequently, in 2019, Lei *et al.* constructed three double bond bridge fluorescence dyes (CX-1, CX-2 and CX-3) with a tunable wavelength at NIR-II (Fig. 9A) [32], and developed a novel probe (probe **13**) by loading CX-1 and CX-3 to micelle. According to this property, these dyes could be used for multicolor imaging *in vivo* at a tissue depth of up to 4 mm (Fig. 9B). Moreover, with the addition of ONOO⁻, the FRET effect between CX-1 and CX-3 is destroyed, resulting in the opposite trend between the emission of CX-1 and CX-3. Therefore, probe **13** can detect ONOO⁻ in ratio. Meanwhile, a credible method was successfully designed to monitor ONOO⁻ levels *in vivo* and used to the assessment of APAP-induced liver injury. As shown in Fig. 9C, the fluorescence intensity of mouse liver treated with APAP was much higher than that of control group and NAC treatment group.

(5) Pyryllum oxidation. Due to the strong electron-withdrawing ability of oxonium, the carbon atom on pyryllum is to nucleophilic attack, which is often regarded as a breakthrough point for preparing ONOO⁻ specific fluorescence probes. Based on this reaction characteristic, Jiang's group developed a NIR ratiometric fluorescence probe (probe **14**) for detecting ONOO⁻ in living cells and mice [33]. Probe **14** structurally

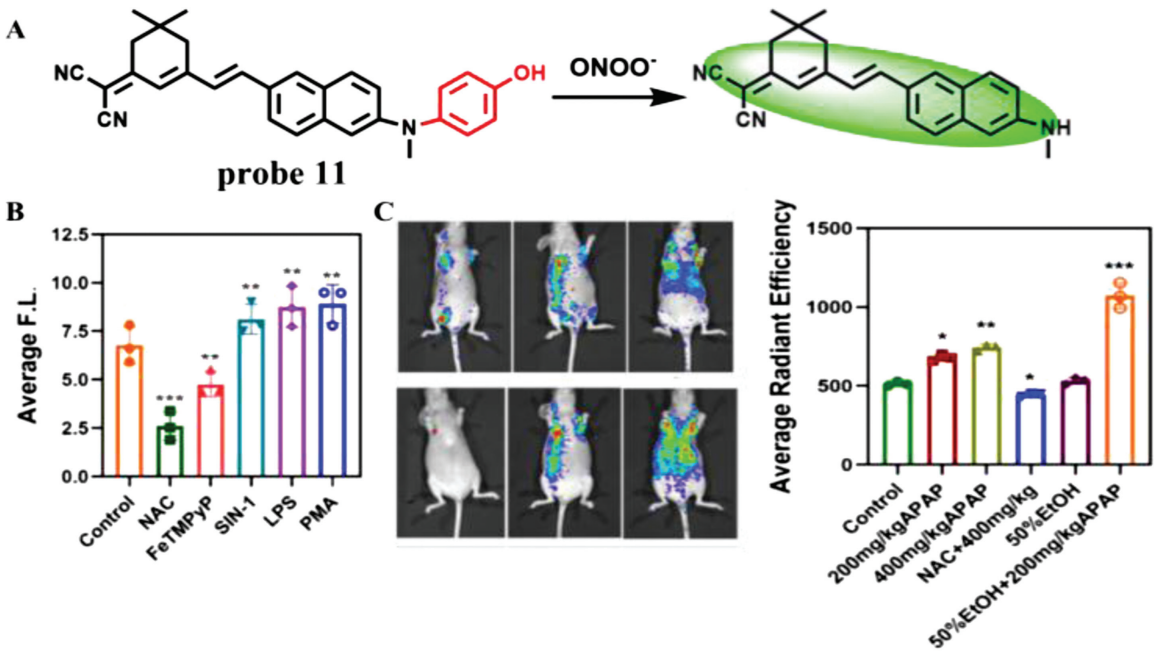

Fig. 7. (A) The reaction mechanism of probe **11** with $ONOO^-$. (B) Fluorescence intensity of LX-2 cells treated with different stimulants. (C) *In vivo* imaging and fluorescence intensity of APAP-induced liver injury mice. Copied with permission [30]. Copyright 2021, Elsevier.

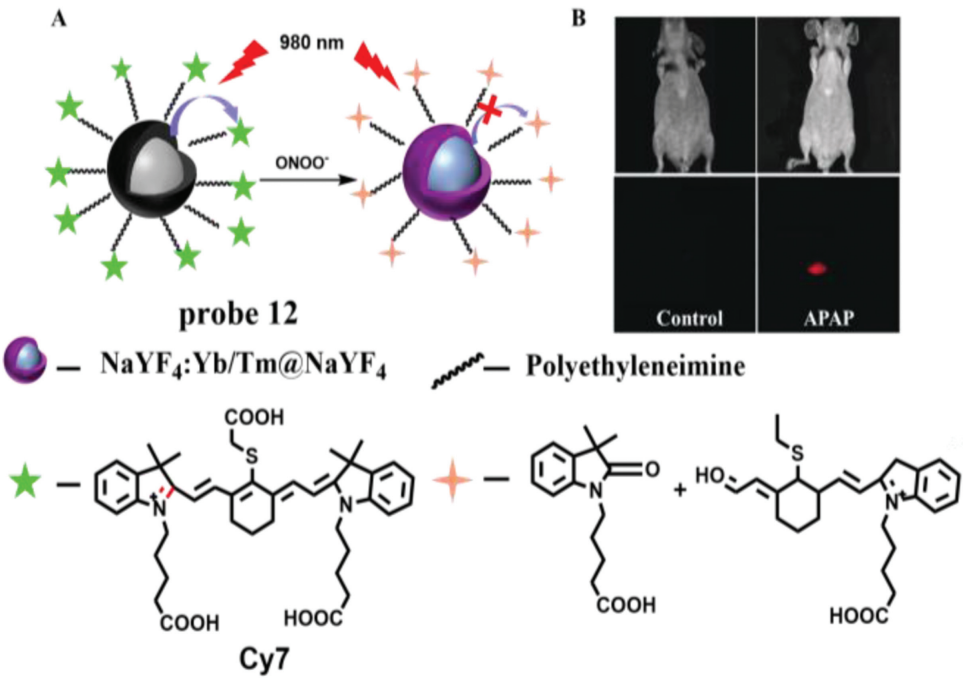

Fig. 8. (A) The reaction mechanism of probe **12** for $ONOO^-$. (B) The images of APAP-induced liver injury in mice. Copied with permission [31]. Copyright 2017, Wiley.

takes a coumarin-benzopyrylium group as a fluorophore and a galactose moiety as hepatocyte-targeting unit (Fig. 10). Due to the extended π-conjugation, probe **14** displayed NIR emission at 720 nm when excited at 440 nm. However, when $ONOO^-$ was added, the strong fluorescence of probe **14** diminished at 720 nm and increased at 500 nm, which was emitted by coumarin 343 acquired from oxidation and cleavage of probe **14**. Therefore, a ratio fluorescence response to $ONOO^-$ could be achieved by a large stokes shift (220 nm), which made probe **14** highly sensitive (LOD = 0.17 μmol/L) and selective. Like probe **10**, probe **14** could specifically target hepatoma cells because of its galactose group. The imaging results in living cells and mice showed that probe **14** could use for assessment of hepatotoxicity induced by APAP and its remediation by using hepatoprotective drugs.

Since some bioactive substance, such as HClO and SO_3^{2-} could bleach the cyanine dyes, leading to a poor selectivity of cyanine dyes to $ONOO^-$. To overcome the problem, Liu *et al.* designed two nanoprobes (probe **15** and probe **16**) by modifying the above UCNPs with pyrylium based small molecular fluorescent probe E-CC and H-CC, respec-

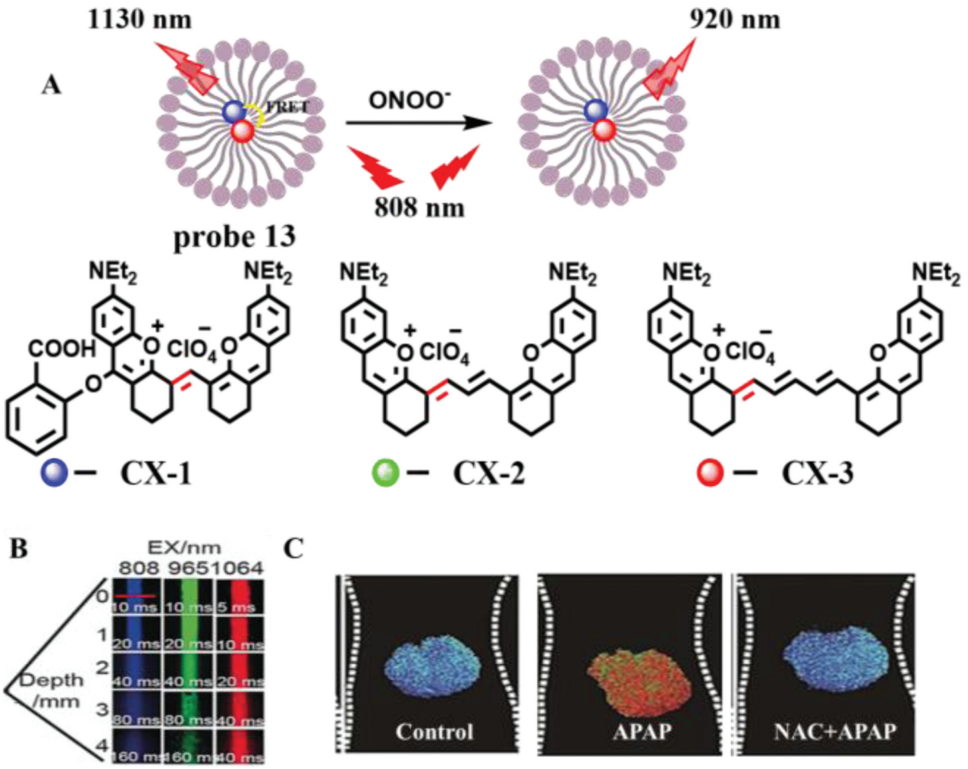

Fig. 9. (A) The reaction mechanism of probe **13** for $ONOO^-$. (B) The penetration depth of fluorescence dyes. (C) The imaging of livers of mice pre-treated with drugs. Copied with permission [32]. Copyright 2019, Wiley.

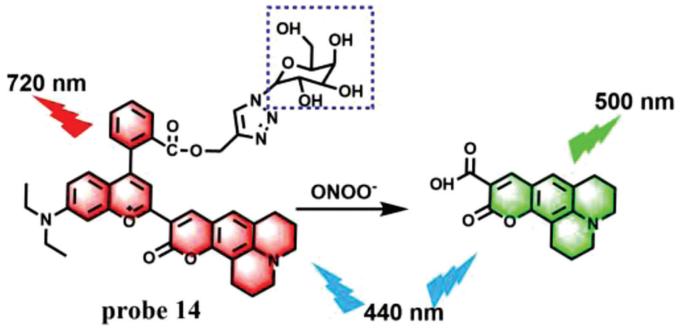

Fig. 10. The reaction mechanism of probe **14** with $ONOO^-$.

tively (Fig. 11A) [34]. The typical emission of UCNPs at 540 nm, 660 nm and 810 nm of probe **15** and probe **16** could be activated by $ONOO^-$, and the ratio of three emissions (I_{540}/I_{660} or I_{660}/I_{810}) could be employed for quantitative measurement (Fig. 11B). Both of the two UCNPs-based probes showed high selectivity toward $ONOO^-$ without interference from HClO and SO_3^{2-}. The LODs of probe **15** and **16** were estimated to be 154 nmol/L and 241 nmol/L, respectively. More importantly, the liver region of mice showed strong fluorescence after CCl_4 treatment (Fig. 11C), which indicated the probe **16** can detect $ONOO^-$ in CCl_4-induced acute hepatotoxicity of mice.

(6) Others. Liu *et al.* developed a fluorescence chemodosimeter (probe **17**) in 2019, in which rhodamine B is used as fluorophore and 1,2-dimethylhydrazine is regarded as a reaction site of $ONOO^-$ (Fig. 12A) [35]. The 1,2-dimethylhydrazine was introduced into the fluorophore to form a spirocyclic ring, which quenched the fluorescence of probe **17**. After the addition of $ONOO^-$, the ring was opened and the fluorescence recovered at 585 nm. Experimental results indicated that compared with other relevant active substances, probe **17** not only had significant specificity for $ONOO^-$, but also could precisely determine nanomolar concentrations of $ONOO^-$ (0–100 nmol/L) with a LOD of 0.68 nmol/L and a fast response time of less than 3 s. Moreover, good biocompatibility enabled probe **17** to monitor intracellular basal and fluctuations of $ONOO^-$ in living cells and zebrafish (Fig. 12B).

Based on the advantages of deep penetration depth and high resolution of two-photon and NIR, Mao *et al.* developed a two-photon probe (probe **18**) with NIR-emission for the detection of $ONOO^-$ in 2021 [36]. Probe **18** took rhodamine as the fluorophore and amide structure as the recognition site (Fig. 13A). When reacted with $ONOO^-$, the probe changed from spirolactam structure to ring opening structure, accompanied by fluorescence from quenching to enhancement at 660 nm. With the concentration of $ONOO^-$ ranging from 50 nmol/L to 10 μmol/L, the fluorescence intensity increased 340 times, and the LOD was 15 nmol/L. Meanwhile, probe **18** was not disturbed by related molecules, indicating that the probe has high sensitivity and selectivity. In addition, probe **18** can detect not only endogenous and exogenous $ONOO^-$ at the cellular level, but also $ONOO^-$ produced by inflammation at the animal level. Confocal scanning imaging of mouse liver tissue showed that the penetration depth of the probe was 204 μm (Fig. 13B). Most importantly, the fluorescence of HepG2 cells increased significantly after APAP treatment, while the fluorescence decreased significantly after APAP pretreatment and trans-1,2-dichloroethylene (*t*-1,2-DCE), *t*-1,2-DCE and NAC treatment, indicating that the probe can detect DILI and its repair process (Fig. 13C).

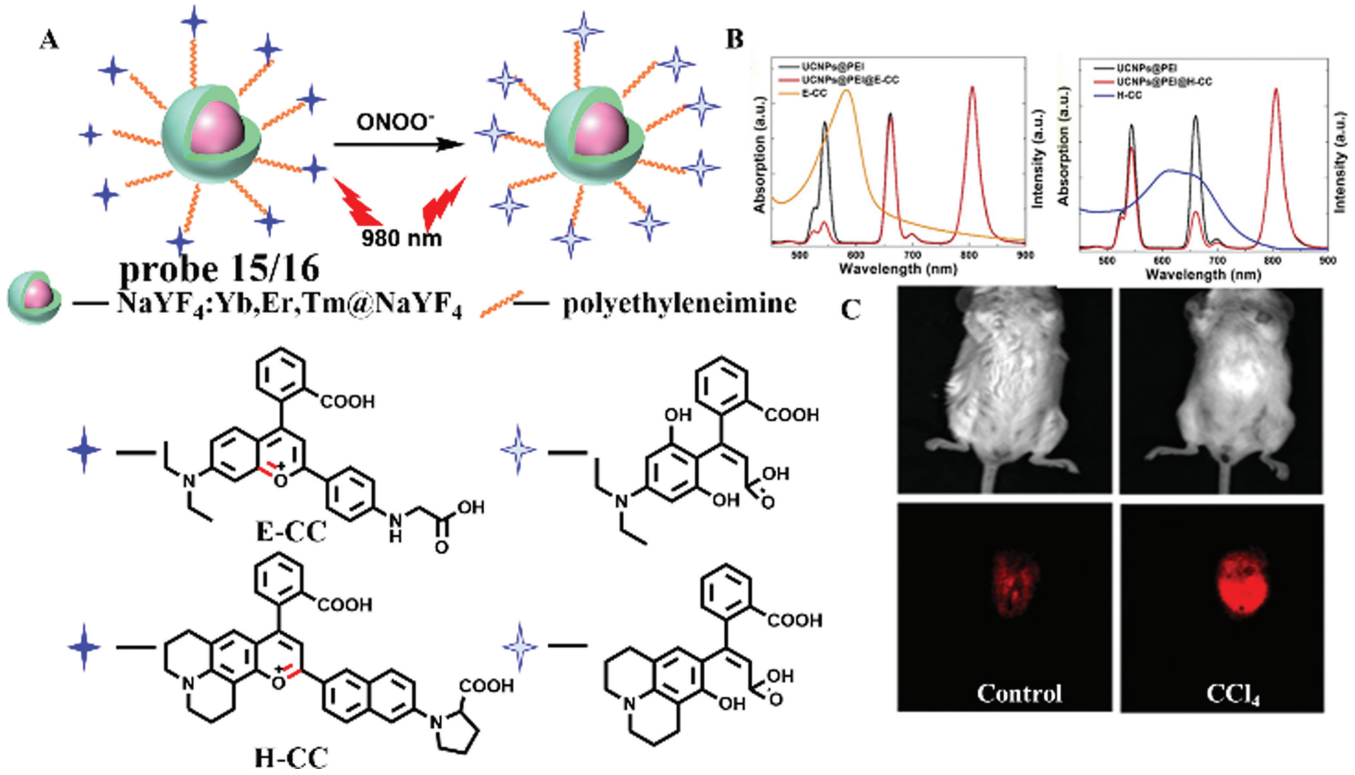

Fig. 11. (A) The reaction mechanism of probe **15** and **16** with $ONOO^-$. (B) The absorption and fluorescence spectra of probe **15** and probe **16**. (C) The images of CCl_4-induced liver injury in mice. Copied with permission [34]. Copyright 2019, Wiley.

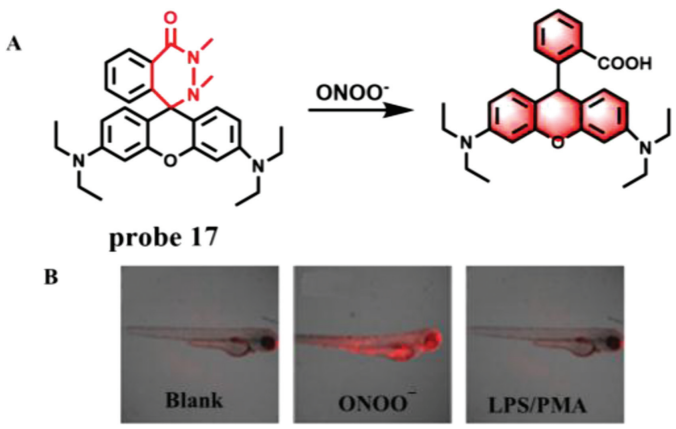

Fig. 12. (A) The reaction mechanism of probe **17** with $ONOO^-$. (B) The fluorescence imaging of zebrafish treated with various drugs. Copied with permission [35]. Copyright 2019, American Chemical Society.

2.2. Detection of NO

As a redox substance, NO is generated in the body under the catalysis of nitric oxide synthase (NOS). Generally, there are three isoforms of NOS, namely neuronal NOS (nNOS), endothelial NOS (eNOS) and inducible NOS (iNOS) [37]. Among them, iNOS only expressed when the cells and/or organ were damaged. Therefore, NO is considered to be another unified, direct and critical biomarker in the early stage of DILI. In 2019, Tang *et al.* developed an activatable organic semiconducting nanoprobe (AOSNP) (probe **19**) [38]. When probe **19** was stimulated by NO, the phenylenediamine derivative was converted to a benzotriazole derivative and its fluorescence red-shifted to NIR-II region (Fig. 14). Probe **19** showed negligible absorption at 808 nm and an insignificant NIR-II fluorescence emission at the wavelength from 900 nm to 1150 nm. However, a remarkable absorption peak at 680 nm appeared and the fluorescence intensity increased about 35-fold in NIR-II with the addition of NO. Meanwhile, the color of the solution changed from yellow to blue-green under natural light. The ratio of emission intensity of probe **19** was positively correlated with the NO concentrations ranging from 0 μmol/L to 35 μmol/L and the LOD was 0.35 μmol/L. Moreover, probe **19** showed no apparent toxicity when it co-incubated with 3T3 cells and HepG2 cells. Animal DILI studies have shown that probe **19** showed excellent passive target to liver and the fluorescence of mouse liver region increased continuously with the extension of time, which proved that the probe could detect NO activity in APAP-induced DILI mice *via* a time-dependent manner.

In 2021, Sun's team constructed a NO-activated nanoprobe (probe **20**) containing D-π-A structure, in which bimethoxyphenylamine-containing dihydroxanthene was used as electron donor, quinoline as receptor and butylamine as recognition group (Fig. 15A) [39]. When NO reacts with butylamine, the absorption peak of the probe red-shifts to 700–850 nm, which can be used for photoacoustic imaging (3D MOST imaging), and the strong emission peak of 910–1110 nm can be used for NIR-II imaging. Probe **20** was used to detect the dynamic changes of NO level in the model of liver injury induced by Triptolide in mice. After Triptolide treatment, the fluorescence of liver region increased gradually with the extension of time (Fig. 15B). Meanwhile, 3D MOST imaging can accurately locate the position and size of the liver in spatial distribution. With the combination of 3D imaging and near-infrared imaging (Fig. 15C), probe **20** can not only monitor the process of liver injury induced by Triptolide, but also monitor the remediation of liver injury, which lays a solid foundation for the clinical detection of liver injury caused by Chinese herbal medicine.

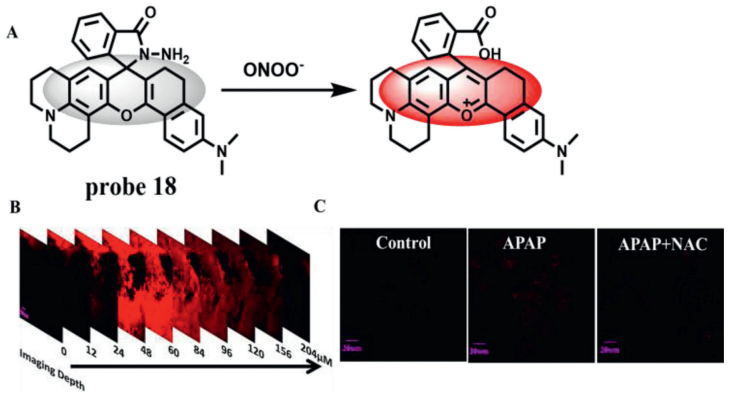

Fig. 13. (A) The reaction mechanism of probe **18** with $ONOO^-$. (B) The Z-scan fluorescence imaging of mouse liver treated with probe **18** and SIN-1. (C) The fluorescence imaging of APAP-induced hepatotoxicity and remediation in HepG2 cells. Copied with permission [36]. Copyright 2021, Elsevier.

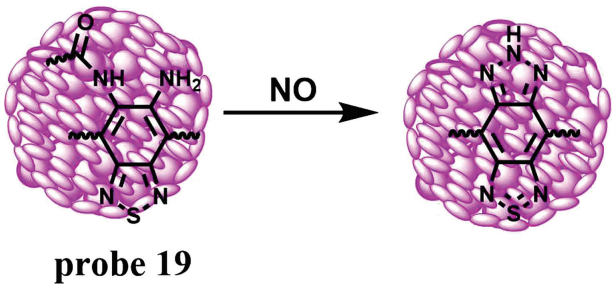

Fig. 14. The reaction mechanism of probe **19** for NO.

2.3. Detection of nitroxyl (HNO)

When acute liver injury occurs, the level of NOS in Golgi and Mitochondria rises sharply, during which will produce a large amount of NO. Since nitroxyl (HNO) is a reductive NO substance, therefore, Wang *et al.* first investigated the relationship between the level of HNO and DILI [40]. In order to overcome the false positive results, they constructed two kinds of targeted fluorescence probes, Golgi-HNO (probe **21**) and Mito-HNO (probe **22**) to image endogenous HNO in living systems, so as to monitor DILI (Figs. 16A and B). In structure, probe **21** and **22** take 2-(diphenylphosphino)-benzoate as the reaction site of HNO and fluorescein and hemicyanine as fluorophores, respectively. In order to achieve Glogi targeting, probe **21** takes bovine serum albumin (BSA) as a Golgi-targeting moiety. When HNO reacted with the probe, ICT effect was caused by inter-molecular attack between adjacent ester molecules, and probe **21** and **22** showed strong fluorescence at 520 nm and 725 nm, respectively. With the concentration of HNO precursor from 0 μmol/L to 30 μmol/L, the LOD of two probes were calculated to be 130 nmol/L and 160 nmol/L, respectively. In addition, animal experiments also confirmed that fluorescence in the mouse liver region was enhanced with the increase of APAP concentration (Fig. 16C), thus revealing a positive correlation between HNO level and DILI degree. Meanwhile, mice injected with the anticancer drug bleomycin showed the same phenomena, suggesting that probe **21** and probe **22** provide double assurance for the diagnosis of DILI.

2.4. Detection of $O_2^{\bullet-}$

As a member of ROS family, $O_2^{\bullet-}$ is produced during cell respiration and plays a fundamental role in cell proliferation and migration. Moreover, O_2^- has the function of immunity and conduction in organism. However, excessive O_2^- level could destroy homeostasis and lead to the occurrence of related disease, such as liver damage and oxidative stress. As an important membrane-bound organelle, endoplasmic reticulum (ER) widely exists in eukaryotic cells and plays an important role in biosynthesis [41–45]. However,

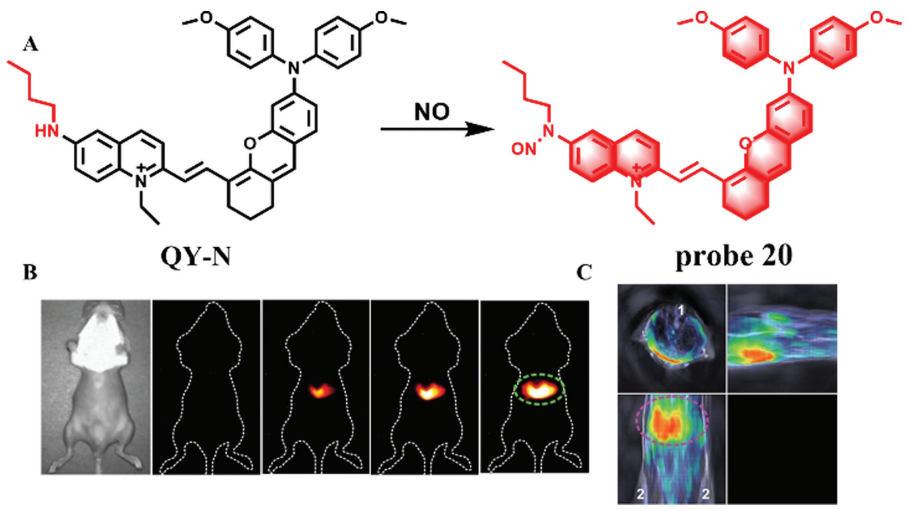

Fig. 15. (A) The reaction mechanism of probe **20** for NO. (B) Imaging of mice pretreated with APAP and injected with probe at different time points. (C) MOST imaging of mice pretreated with APAP and injected with probe. 1–Spinal cord, 2–Hind limbs. Copied with permission [39]. Copyright 2021, Wiley.

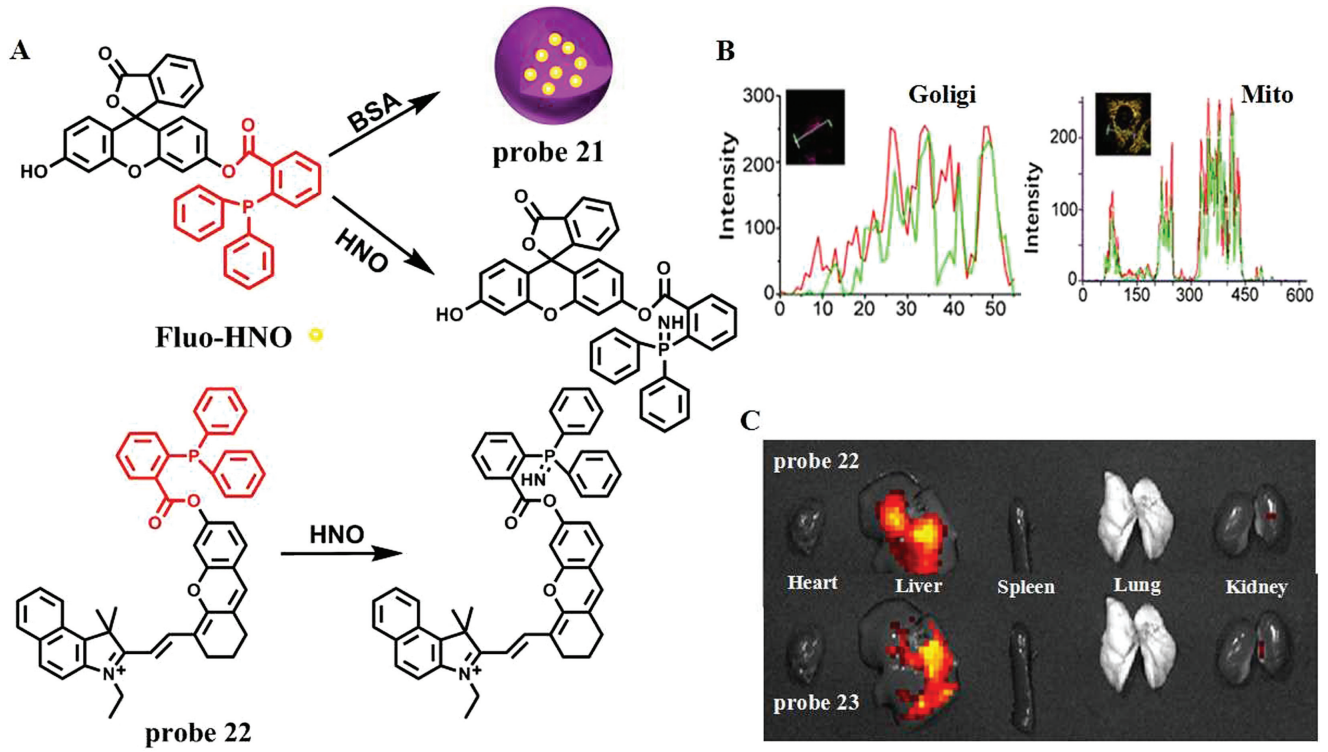

Fig. 16. (A) The reaction mechanism of probe **21**/**22** for HNO. (B) The co-localization imaging of probe and commercial dye in Hela cells. (C) Tissue imaging of DILI by APAP in mice. Copied with permission [40]. Copyright 2021, American Chemical Society.

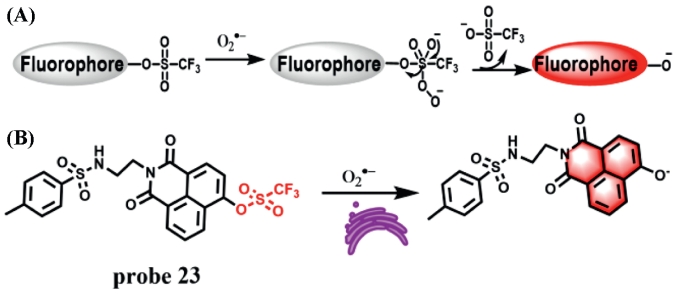

Fig. 17. (A) Proposed reaction mechanism of probe based on TFMS group to $O_2^{\bullet-}$. (B) The reaction mechanism of probe **23** for $O_2^{\bullet-}$.

in pathological state, ER stress usually occurs as the cells are disturbed, during which a variety of ROS can be formed, such as $O_2^{\bullet-}$ [46]. Current biomedical researches have shown that ER is involved in DILI [47]. Therefore, it is of great significance to trace $O_2^{\bullet-}$ level changes *in vivo*.

Trifluoromethanesulfonate (TFMS) group showed good reactivity and selectivity to $O_2^{\bullet-}$ [48], which has been widely employed in the design of $O_2^{\bullet-}$ responsive fluorescent probes by combination with the protection and de-protection strategy and hydroxyl functioned fluorophores [49,50]. As shown in Fig. 17A, the hydroxyl group of the 1,8-naphthalimide fluorophores was protected by TFMS group, leading to the quenched fluorescence due to the decrease of ICT effect of the probe. After reaction with $O_2^{\bullet-}$, the hydroxyl group of 1,8-naphthalimide fluorophore was deprotected, which resulted in strong ICT effect and restoring the strong fluorescence. Based on this reaction mechanism, Zuo *et al.* first developed an ER-targeted TPE probe (probe **23**) for detection of $O_2^{\bullet-}$ (Fig. 17B) [51]. In the structure of probe **23**, the group of naphthlimide is used as an ER-targeted unit, and the fluorophore naphthlimide containing hydroxyl group is selected as fluorescence reporter. Probe **23** itself shows weak fluorescence at 554 nm, while the fluorescence intensity at the same wavelength increased remarkably with the increase of $O_2^{\bullet-}$ concentrations (0–60 μmol/L). The LOD was determined to be 0.33 μmol/L. Moreover, the probe presents high selectivity to $O_2^{\bullet-}$ and low cytotoxicity. Cell experiments demonstrated that probe **23** could be used to image ER $O_2^{\bullet-}$ in living cells visualize the change of $O_2^{\bullet-}$ levels in DILI diseases.

2.5. Detection of HClO

HClO, a member of the highly ROS family, is generated from the myeloperoxidase (MPO) catalyzed the oxidation reaction between chloride and H_2O_2 [52]. Typically, HClO regulates the basic functions for immune response in human being during pathogen invasion [53]. However, dysregulation of HClO *in vivo* can cause tissue and organ injury, and even some diseases related to neurodegenerative diseases, inflammatory diseases and cancer [54–56]. Therefore, monitoring the fluctuation of HClO is vital. Generally, selenide can be easily oxidized by HClO to form selenoxide, which makes the selenide-containing probe display turn-on fluorescence change [57,58]. Subsequently, the selenoxide can undergo a self-generated *syn* elimination to produce α,β-unsaturated ketone. Nowadays, this oxidation/elimination tandem reaction has been used to restore the fluorescence of coumarin in HClO probes [59,60]. According to this reaction mechanism, Xie's group first designed a two-photon ratio type fluorescence probe Coum-Se (probe **24**) for monitoring HClO [61]. In structure, probe **24** consisted of a coumarin fluorophore and an α-phenylseleno carbonyl moiety, and emitted green fluorescence at 495 nm (Fig. 18). With the addition of HClO, the initial emission band of probe **24** reduced progressively and a new emission peak emerged at around 618 nm, which was caused by the conversion of probe structure from Coum-Se to Coum-NIR. The fluorescence ratio of I_{618}/I_{495} increased with the increasing concentrations of HClO and gave a good linear relationship between the ratio and HClO concentrations (0–20 μmol/L, LOD = 4.6 nmol/L). More-

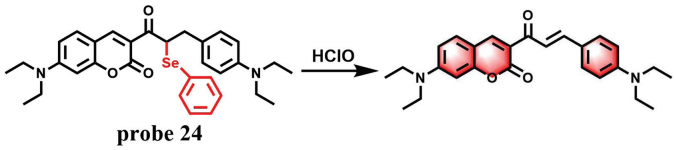

Fig. 18. The reaction mechanism of probe **24** with HClO.

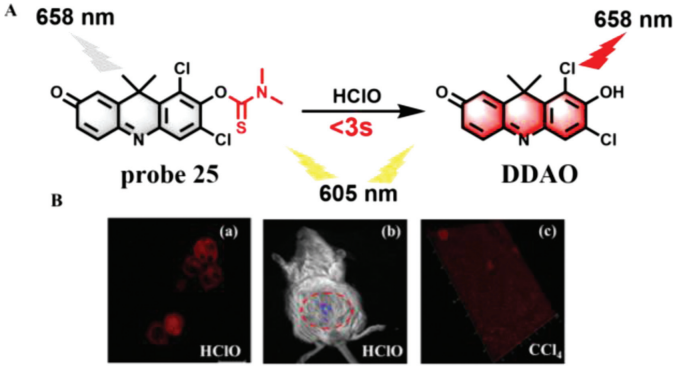

Fig. 19. (A) The reaction mechanism of probe **25** for HClO. (B) The imaging of probe **25** in (a) MCF-7 cells, (b) mice and (c) liver tissues. The circled part indicates liver. Copied with permission [62]. Copyright 2020, Elsevier.

over, probe **24** could be used to visualize of HClO fluctuation in both live cells and animals.

Recently, Deng and co-workers used DDAO (6,8-dichloro-7–hydroxy-9,9-dimethylacridin-2(9*H*)-one) as a NIR fluorophore and developed a new colorimetric NIR probe (DDAO-ClO) (probe **25**) for detection of HClO (Fig. 19A) [62]. Probe **25** itself has almost no fluorescence when the excitation wavelength was set at 605 nm. However, upon reaction with HClO, probe **25** was converted to DDAO, which could emit obvious NIR fluorescence at 658 nm and could selectively image HClO in biological systems with fast response (less than 3 s) and high sensitivity (LOD = 7.3 nmol/L). As shown in Fig. 19B, probe **25** could real-time monitor the change of HClO levels in MCF-7 cells and mice. Meanwhile, 3D imaging showed that the fluorescence of mouse liver tissues was significantly enhanced after they treated with CCl_4.

2.6. Detection of H_2O_2

As one of the importance of ROS, H_2O_2 regulates the redox signal in many physiological processes, such as oxidative stress and angiogenesis [63,64]. *In vivo*, H_2O_2 is mainly produced in liver by O_2^- under the action of peroxidase [65]. The increase of H_2O_2 level will lead to liver damage and necrosis [66]. Therefore, H_2O_2 is often used as an important indicator for evaluation of DILI. In 2020, Jiang's team synthesize a ratio type NIR fluorescence probe (probe **26**) for H_2O_2 with galactose as a hepatocyte-targeting group and coumarin pyran as a fluorophore [67]. As expected, probe **26** exhibited NIR emission at 706 nm. With the addition of H_2O_2, the oxidative cracking of probe **26** reduces π-conjugation of the structure, which was accompanied by a blue-shift of fluorescence emission from 706 nm to 482 nm (Fig. 20A). Therefore, a ratiometric fluorescence response toward H_2O_2 (F_{482}/F_{706}) could obtain large emission shift (224 nm) (Fig. 20B), which led to excellent selectivity and sensitivity. A good linear relationship between the ratio and H_2O_2 concentrations from 1.0 μmol/L to 50.0 μmol/L was obtained and the LOD was estimated to be about 0.33 μmol/L. In addition, probe **26** was used to monitor the up regulation of H_2O_2 during drug-induced hepatotoxicity in HepG2 cells. What's more, probe **26** could precisely target the zebrafish liver and accurately detect the level of H_2O_2 in liver (Fig. 20C).

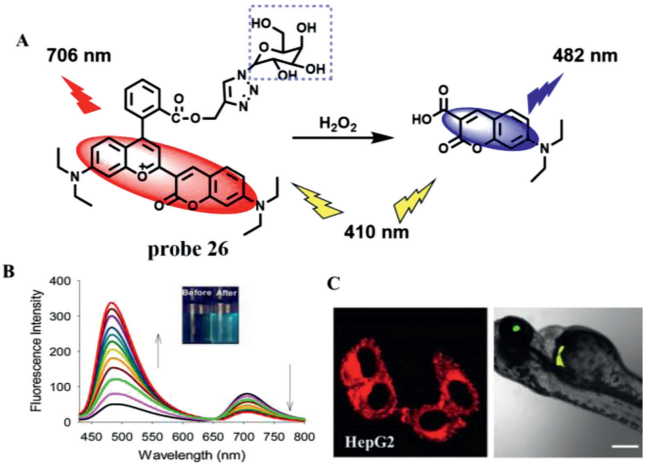

Fig. 20. (A) The reaction mechanism of probe **26** for H_2O_2. (B) Fluorescence spectra of probe **26** after adding different H_2O_2 concentrations. (C) Fluorescence imaging of probe **26** in HepG2 cells and zebrafishes. Copied with permission [67]. Copyright 2020, Elsevier.

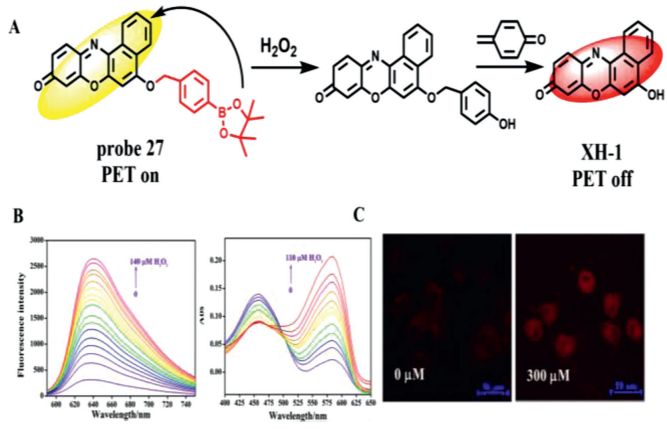

Fig. 21. (A) The reaction mechanism of probe **27** with H_2O_2. (B) Fluorescence and absorption spectrum of probe after addition of H_2O_2. (C) Imaging of HepG2 cells treated with probe in the absence ad presence of APAP. Copied with permission [68]. Copyright 2021, Elsevier.

In 2021, Xu's team used borate as the recognition group and XH-1 as the fluorophore to develop a new probe (probe **27**) for detecting H_2O_2 with dual signals of fluorescence and colorimetry for the first time (Fig. 21A) [68]. After adding H_2O_2, the strong absorption peak at 455 nm red-shifted to 585 nm, and could be judged by naked eye colorimetry. At the same time, the probe had a weak emission peak at 638 nm (Fig. 21B). With the addition of hydrogen peroxide concentration from 0 μmol/L to 140 μmol/L, the borate group fell off, the PET effect was inhibited, the fluorescence at 638 nm was gradually enhanced, and the LOD was 91 nmol/L. Probe **27** further confirmed its universality by detecting H_2O_2 in serum by spiked recovery experiment and indirectly detecting glucose by fluorescence method. Moreover, probe **27** can not only detect endogenous and exogenous H_2O_2 in HepG2 cells, but also effectively monitor H_2O_2 level during DILI in HepG2 cells (Fig. 21C).

Optoacoustic (OA) imaging can avoid the photon scattering of biological tissue, while NIR imaging has a certain penetration depth and low fluorescence background. The combination of these two imaging methods can better realize the monitoring *in vivo*. Chen *et al.* combined photoacoustic imaging and near infrared imaging, and developed a probe (probe **28**) for monitoring the changes of H_2O_2 level in the process of DILI induced by isoniazid (INH) [69]. Probe **28** was mainly composed of a tricyanofuran-containing heptamethine as the chromophore and a nitrophenoxy-

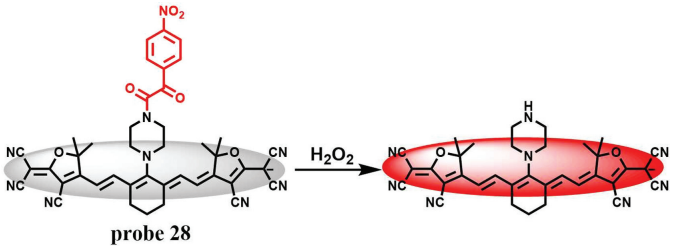

Fig. 22. The reaction mechanism of probe **28** with H_2O_2.

acetamide as the recognition group (Fig. 22). Due to the PET effect between the recognition group and heptamethylamine, probe **28** itself was weak. In the presence of H_2O_2, the absorption peak shifted red from 680 nm to 755 nm, and the fluorescence was enhanced 10 folds at 920 nm. Meanwhile, probe **28** had high sensitivity to H_2O_2 and was not disturbed by related substances. Most importantly, probe **28** can effectively monitor the level of H_2O_2 in the process of INH induced liver injury in mice through NIR imaging and OA imaging, and verify the authenticity and effectiveness of the probe in the monitoring of DILI through histological experiments.

2.7. Detection of $^{\bullet}OH$

The hydroxyl radical ($^{\bullet}OH$) is the strongest oxidant agent among ROS, and excessive exposure of $^{\bullet}OH$ not only causes lipid peroxidation and cell membrane damages, but also interacts with different proteins to destroy the functions of receptors and enzymes [70]. More importantly, excessive $^{\bullet}OH$ can cause irreversible oxidative damage to DNA [71]. Therefore, it is of clinical significance for preventing the further development of liver injury to detect timely and accurately the level of $^{\bullet}OH$ in the process of DILI. Based on FRET effect, Ma *et al.* combined thiolated single DNA strand labelled with carboxyfuorescein and thiolpoly(ethylene glycol)$_{2000}$-galactose onto the surface of gold nanoparticles (AuNPs) to develop an $^{\bullet}OH$-responsive and hepatocyte-targeted nanoprobe (probe **29**) (Fig. 23A) [72]. Due to FRET effect, the fluorescence of probe **29** at 520 nm was quenched by AuNPs completely. However, when $^{\bullet}OH$ was added, the Thymine-Thymine (TT) sequence in DNA strand could be cleaved by $^{\bullet}OH$ and then the FAM was released from probe **29**, resulting in strong emission at 520 nm (Fig. 23B). Meanwhile, owing to the strong affinity of PEG$_{2000}$-GAL with asialoglycoprotein receptor (ASGPR)-rich hepatocyte, the fluorescence intensity on hepatocyte membrane increased progressively with the increase of APAP concentrations, as well as incubation time (Fig. 23C). A similar result can be seen in triptolide-induced liver injury. These results demonstrated that probe **29** could be applied to visualize the level of $^{\bullet}OH$ during DILI.

2.8. Detection of GSH

GSH is an important thiol in the organism, which plays a critical role in maintaining redox balance of body. When GSH can not timely combine with a large number of active metabolites generated by overdose of drugs in liver, it will cause serious DILI. Therefore, GSH plays an important role in detoxification. In 2014, Yin group developed a cyanine-based NIR fluorescence probe (probe **30**) with high selectivity for GSH and good permeability (Fig. 24A) [73]. The fluorescence was significantly decreased after Hela cells were incubated with *N*-methylmaleimide (NMM) and probe 30. However, the fluorescence recovered when the cells were treated with GSH. Meanwhile, probe **30** can detect the GSH level in various tissues directly. The fluorescence intensity decreased remarkably in some tissues (such as liver, lung, kidney and spleen) under the stimulation of excessive APAP, indicating that the GSH level in the injured tissues induced by APAP decreased significantly (Figs. 24B and C). Subsequently, Chen's team made a breakthrough in the previous design of probes for detecting GSH based on the strong nucleophilicity of mercaptan. They synthesized successfully a NIR GSH specific fluorescence probe **31** by theoretical calculation [74]. As shown in Fig. 25A, the fluorescence of fluorophore BODIPY derivative was masked by PET effect. However, when probe **31** reacted with GSH, the recognition group was converted to phenol, and thus the fluorescence of probe **31** was restored and enhanced about 45-fold at 663 nm. From titration experiment, the fluorescence intensity of probe **31** had a good linear relationship with GSH concentrations (0–100 μmol/L, LOD = 83 nmol/L). Moreover, the imaging results suggested that probe **31** could not only effectively detect the change of GSH level in NCI-H1975 cells before and after α-LPA treatment (Fig. 25B), but remarkably decreased the fluorescence intensity in the tissues of mice treated with APAP (Fig. 25C), indicating that design concept of probe **31** could not only visually detect GSH fluctuations in cells and tissues, but pave the way for future "trial-and-error" method. However, the response time (20 min) was not conducive to real-time detection of DILI samples.

2.9. Detection of enzymes

As an essential hydrolase, ALP can hydrolyze specifically phosphate groups. Recent studies have shown that the ALP activity increases dramatically with the emergence of DILI. Although detection of ALP level may cause some inaccuracy in clinical, ALP is still regarded as one of the important markers to evaluate DILI. In 2015, a ratiometric fluorescence probe (probe **32**), which was synthesized by adding a phosphate group and an amine-*N*-oxide group to a 1,8-naphthalimide derivative, was developed for detection of ALP by Hou team (Fig. 26) [75]. Without ALP, probe **32** itself shows a typical emission peak at 468 nm for the naphthalimide substituted with phosphate group. With the addition of ALP, the phosphate group was cleaved into a-OH with stronger electron donating ability, accompanied by a new emission peak at around 554 nm, which was corresponded to the emission of naphthalimide derivatives substituted by −OH at the 4th position. Meanwhile, the emission intensity ratio (F_{554}/F_{468}) increased with the increase of ALP amount and showed a linear relationship between 0.5 U/L and 5.0 U/L with a LOD of 0.38 U/L. *In vivo* imaging experiments of zebrafish showed that the fluorescence intensity of probe **32** reached a stable state after incubation of 1 h, and probe **32** was gradually excreted from zebrafish without accumulation after 24 h, indicating that probe **32** had good biocompatibility. The results of drug-induced experiment in zebrafish showed that with the increase of APAP concentration and incubation time, the blue fluorescence intensity decreased progressively and the green fluorescence increased at the same time, suggesting that APAP could obviously give rise to the elevation of ALP level, which resulted from drug-induced organ injury. A similar result can be found in carbon tetrachloride (CCl_4)-induced zebrafish larvae.

LAP is an essential metallopeptidase, which is closely related to many diseases, such as tumor, kidney injury and liver injury. In recent years, a series of LAP-specific fluorescence probes have been developed for assessment of DILI. According to the ability of LAP to hydrolyze N-terminal leucyl groups (Fig. 27A), He *et al.* developed a LAP-specific fluorescence probe (HCAL, probe **33**), which is synthesized by conjugation of amino group of a NIR hemicyanine (HCA) with carboxyl group of leucine (Fig. 27B) [76]. Probe **33** itself displays a strong absorption peak at 598 nm and rather weak fluorescence. However, after addition of LAP, the absorption peak of probe **33** is red-shifted from 598 nm to 670 nm and fluorescence enhancement appears at 705 nm. There exists a good linear relationship between the fluorescence intensity and LAP

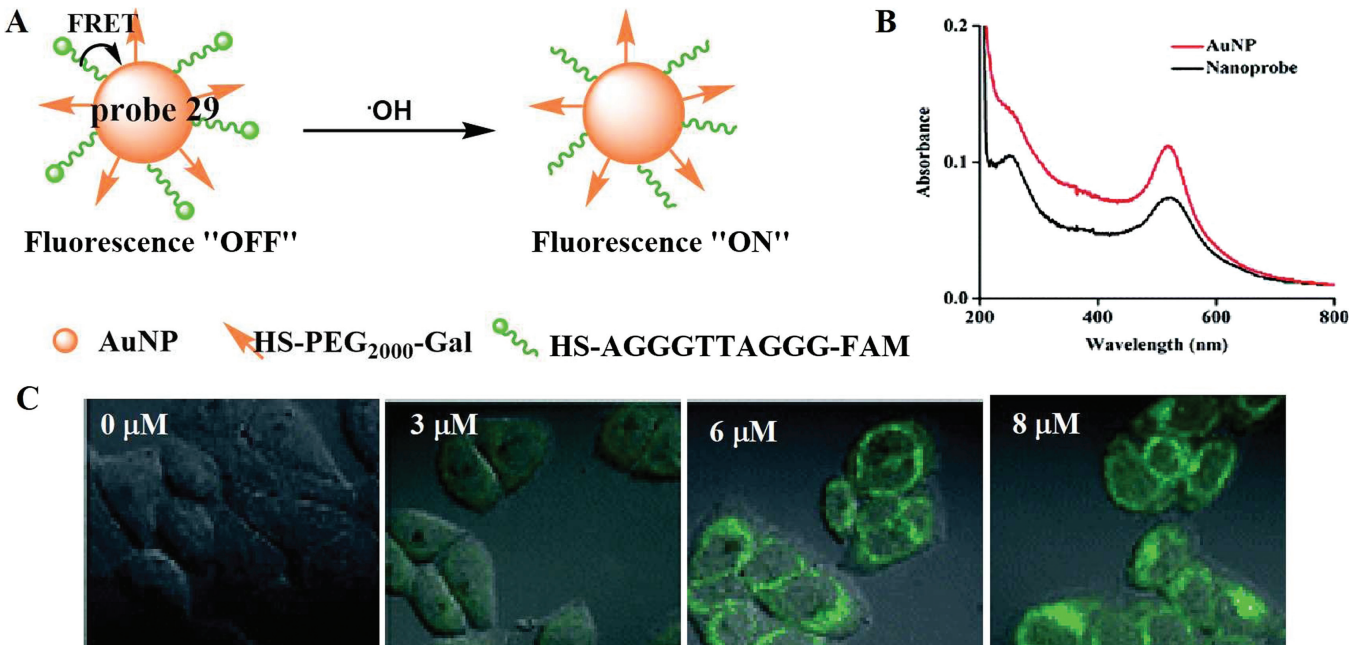

Fig. 23. (A) The reaction mechanism of probe **29** for ·OH. (B) The absorption spectra of probe **29**. (C) Fluorescence imaging of LO2 cells treated with different APAP concentrations. Copied with permission [72]. Copyright 2018, Royal Society of Chemistry.

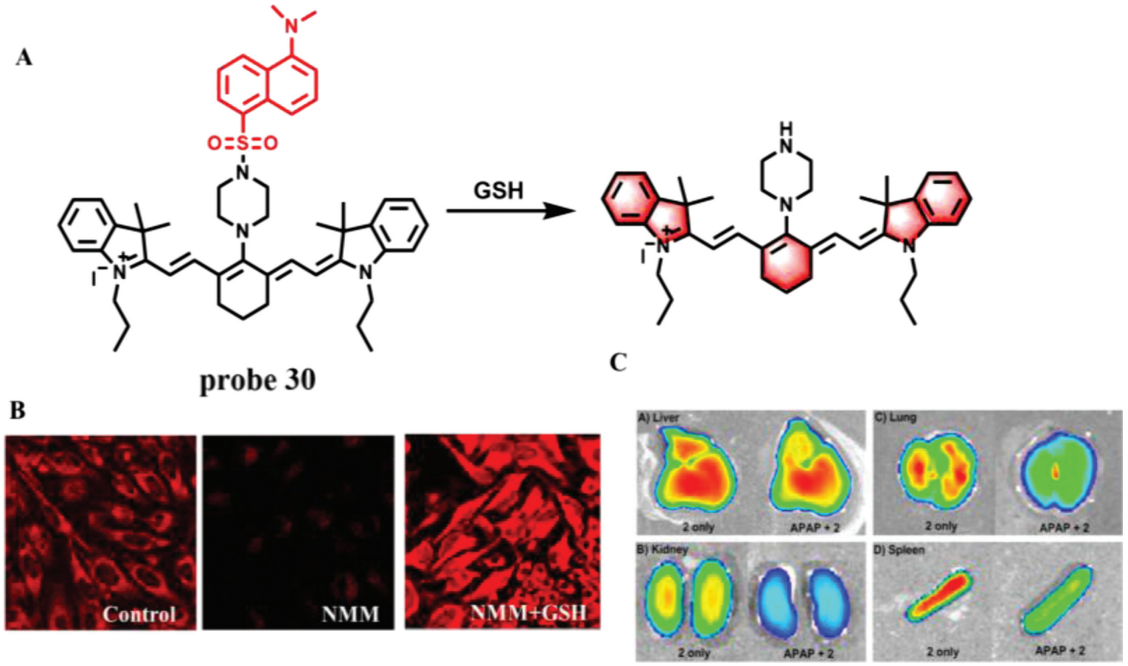

Fig. 24. (A) The reaction mechanism of probe **30** with GSH. (B) Fluorescence imaging of probe **30** in HeLa cells. (C) The images of different tissues from mouse injected with or without APAP. Copied with permission [73]. Copyright 2014, American Chemical Society.

concentrations ranging from 1 U/L to 50 U/L. The LOD is found to be 0.19 U/L. Probe **33** can enhance the fluorescence in LO2 and HepG2 cells pre-treated with Ace in a dose- and time-dependent manner, while this enhancement can be inhibited remarkably by bestatin, which indicates that the LAP level is up-regulated in the DILI model. Moreover, the same results were also found in Ace-induced mice and HepG2 tumor xenografted mice. Subsequently, several fluorescence probes with similar reaction mechanism were developed for detection of LAP in DILI, such as probe **34** (Fig. 27C) [21] and probe **35** (Fig. 27D) [77].

In 2021, Yang's team developed a highly selective red fluorescence probe (probe **36**) using alanine as the reactive group of LAP for the first time (Fig. 28A) [78]. Probe **36** had strong emission peak at 569 nm. With the addition of LAP concentration from 0 U/L to 50 U/L, the fluorescence intensity at 617 nm gradually increased, and the concentrations of LAP were proportional to the ratio of $F_{617\ nm}/F_{569nm}$ with a LOD of 0.2 U/L. Meanwhile, with good water solubility and cell membrane penetration, probe **36** had been successfully applied to the biological imaging of cells and zebrafish (Fig. 28B), which indicated that probe **36** could monitor

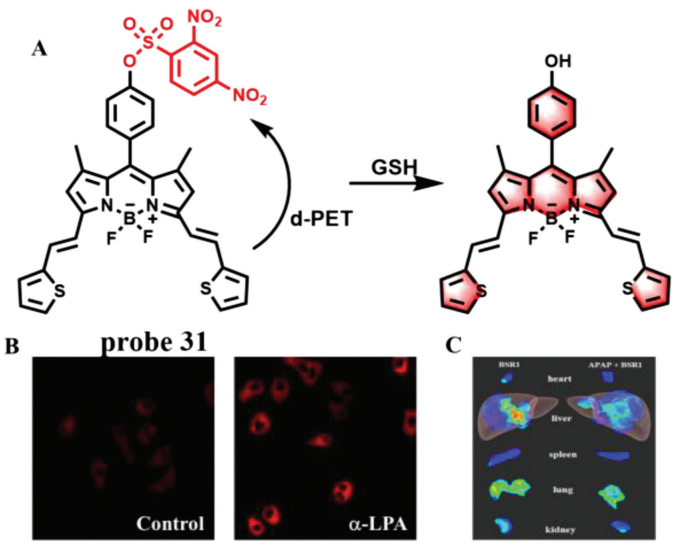

Fig. 25. (A) The reaction mechanism of probe **31** with GSH. (B) Confocal microscopy images of NCI-H1975 cells treated with probe in the absence and presence of α-LPA. (C) *In vivo* images of the tissues incubated with or without APAP. Copied with permission [74]. Copyright 2019, American Chemical Society.

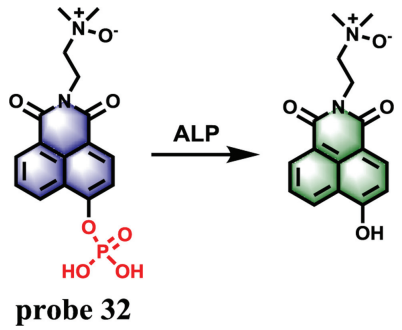

Fig. 26. The reaction mechanism of probe **32** for ALP.

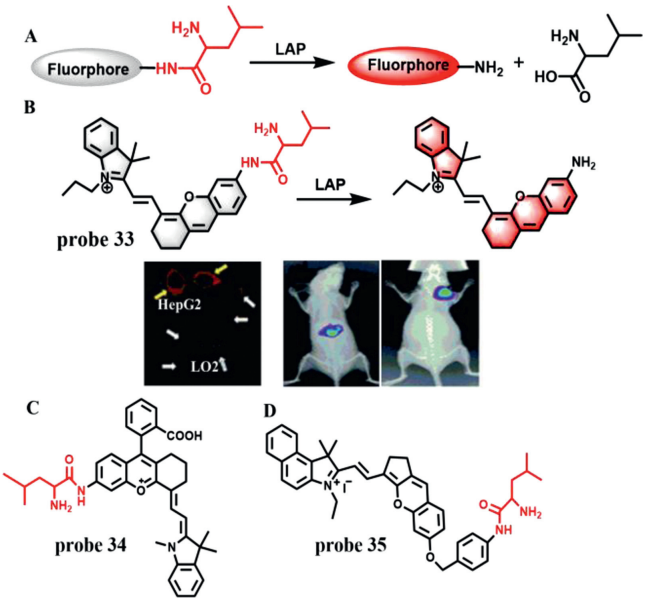

Fig. 27. (A) The mechanism of fluorescent probes for the detection of LAP. (B) The reaction mechanism of probe **33** for LAP and the confocal fluorescence images of different cells, mice and HepG2 tumor xenografted mice. (C) The structure of probe **34**. (D) The structure of probe **35**. Copied with permission [76]. Copyright 2017, Royal Society of Chemistry.

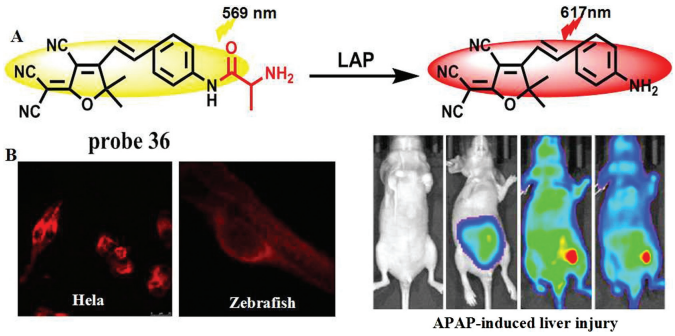

Fig. 28. (A) The reaction mechanism of probe **36** with LAP. (B) The images of probe **36** in living cells, zebrafish and mouse. Copied with permission [78]. Copyright 2021, Elsevier.

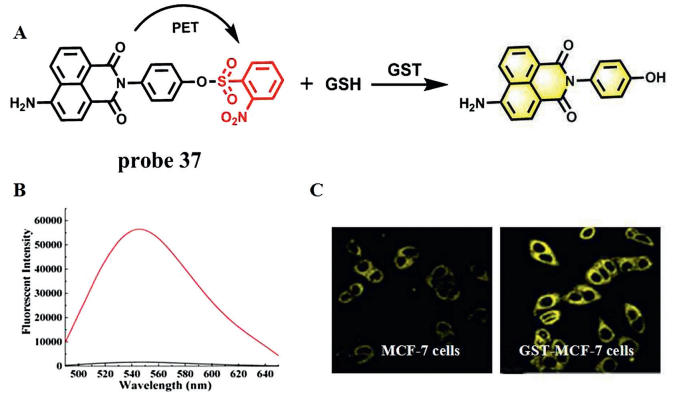

Fig. 29. (A) The reaction mechanism of probe **37** with GST. (B) Fluorescence spectra of probe **37** with GST in the presence of GSH. (C) Fluorescence images of MCF-7 cells and GST-MCF-7 cells without NMM. Copied with permission [82]. Copyright 2017, American Chemical Society.

the changes of ALP in mouse liver injury model in real time, and become a promising ALP tracer tool.

Glutathione S-transferase (GST) mainly exists in the cytoplasm of liver. It can reduce toxicity and promote urinary excretion by catalyzing the binding of GSH with reactive metabolites in liver [79,80]. When the liver is seriously damaged, GST and GSH will be released from the liver cytosol, resulting in the decrease of the GST activity in liver cytosol [81]. In 2017, Zhang *et al.* used naphthalimide derivative with efficient TP property as a fluorophore and a 2,4-dinitrobenzenesulfonate group as GST recognition group and fluorescence quencher to synthesize a GST-specific TP fluorescence probe (P-GST, probe **37**) (Fig. 29A) [82]. In the absence of GST, the emission of the fluorophore is quenched by 2,4-dinitrobenzenesulfonate group due to PET effect. However, when GST and GSH were present, the GST promoted the sulfhydryl group of GSH to attack the electrophilic moiety on the recognition group, thereby removing the recognition unit from probe **37** and releasing the TP fluorophore, accompanied by a 40-fold fluorescence enhancement at 550 nm (Fig. 29B). The application of probe **37** in living cells and animal model of liver injury showed that probe **37** could be used as a tool for detecting and imaging GST level in cells and DILI samples (Fig. 29C).

GGT is a kind of protease that binds to cell membrane and regulates intracellular GSH homeostasis. It is reported that the endogenous GGT level can accurately reflect the state of the liver. Therefore, GGT is generally regarded as a preclinical and clinical indicator of DILI and has been attracted great attention [83]. Zhang group designed a TP fluorescence probe **38** by connecting a glutamic acid with a dicyanomethylene-4*H*-pyran derivative to detect GGT in biological samples with a LOD of 0.057 U/L (Fig. 30A) [84]. The γ-glutamyl amide moiety could be cleaved in the presence of

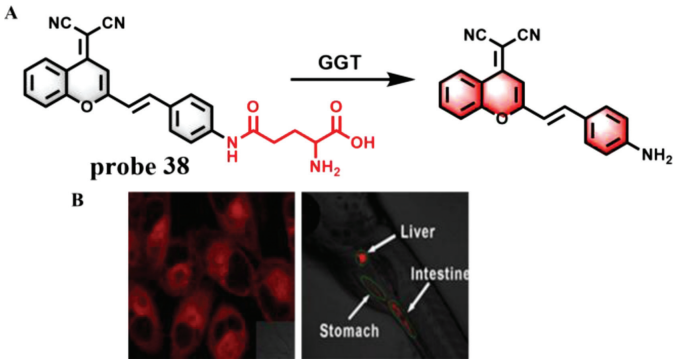

Fig. 30. (A) The reaction mechanism of probe **38** with GGT. (B) The images of probe **38** in A2780 cells and zebrafish. Copied with permission [84]. Copyright 2016, Elsevier.

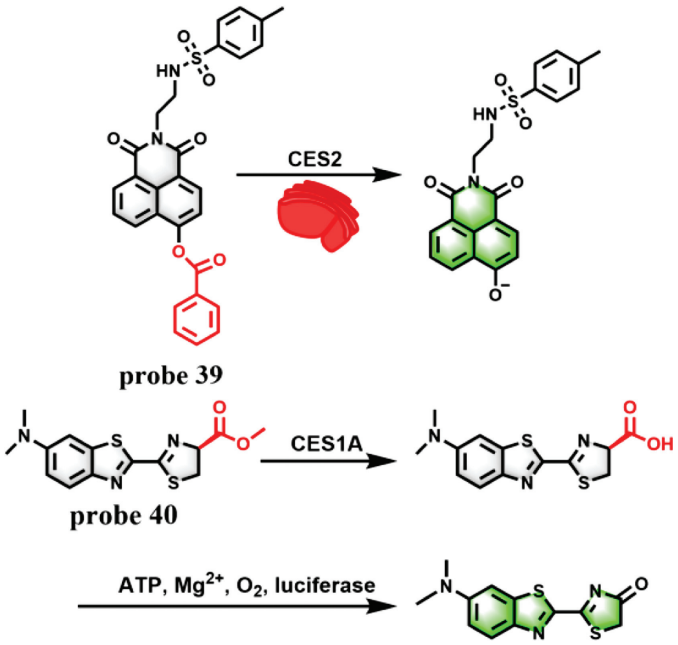

Fig. 31. The reaction mechanism of probe **39** and probe **40** for CES2 and CES1A, respectively.

GGT, which led to a large fluorescence enhancement at 635 nm. Interestingly, probe **38** could be used as a potential tool to evaluate the overexpressed level of GGT in DILI samples (Fig. 30B). In addition, considering that carboxylesterase plays a critical role in metabolism of various endogenous substances and detoxification of clinical drugs, two fluorescence probes including probe **39** [85] and probe **40** [86] have been synthesized for detection of carboxylesterase 2 (CES2) and carboxylesterase 1A (CES1A) to evaluate DILI, respectively (Fig. 31).

2.10. Detection of ATP

ATP, as an endogenous danger signal, automatically initiates immune and inflammatory responses when cells are under stress. Based on the advantages of high signal-to-noise ratio and deep penetration of near-infrared two-region fluorescent probe, Ren *et al.* designed a novel cyanine fluorescent dye (Fig. 32A) [87], which has better photostability and chemical stability than commercial IR1061 and indocyanine green, and has a large stokes shift and anti-solvation effect. At the same time, Ren's team introduced carboxylic acid groups to construct fluorescent dye NIRII-RT4, and rationally designed a series of activated fluorescent probes (probes

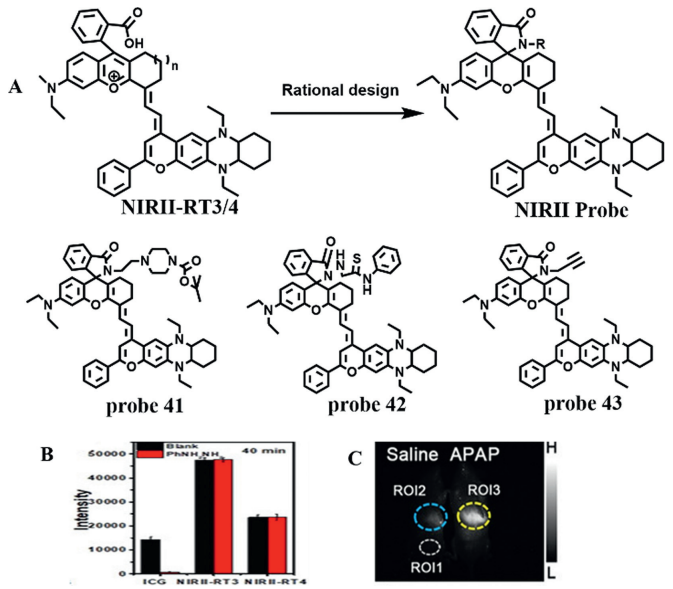

Fig. 32. (A) Design idea of probe. (B) Comparison of fluorescence intensity between commercial NIR probe ICG and NIRII-RT3/4 in liver of Kunming mice after hemolysis drug administration. (C) The fluorescence imaging of mice treated with APAP. ROI1represents background area, and ROI2/ROI3 represents the liver area of mice. Copied with permission [87]. Copyright 2020, Wiley.

41/**42**/**43**) by switching structure of spiral rings (Fig. 32B), which are the responses to adenosine triphosphate (ATP), pH and mercury. Here, probe **41** was selected to monitor the process of drug-induced liver injury in real time. The fluorescence intensity of probe **41** at 918 nm increased continuously with the increase of ATP content from 0 mmol/L to 2 mmol/L, and showed a good linear relationship. In addition, probe **41** has high selectivity for ATP. Moreover, when mice were given probe **41** after liver injury induced by APAP, the liver showed obvious fluorescence with the extension of time (Fig. 32C). At the same time, the liver injury induced by CCl_4 is consistent with the above phenomenon. The above phenomena not only confirm that probe **41** can monitor the process of drug liver damage in real time, but also reflect the fluctuation of ATP in the process.

2.11. Detection of two markers

Due to the complexity of sample environment, detection of single marker for evaluation of DILI often results in inevitable errors. To improve the accuracy of DILI detection, a probe to detect multiple markers at the same time is a main direction of DILI probe design. Recently, several probes designed for two markers were developed for evaluation of DILI.

As a kind of ROS, HCIO can remove pathogens in the body and avoid the invasion of external bacteria under normal conditions [88]. However, excessive HCIO will injury organism and tissue damages. Meanwhile, NAC can promote the production of H_2S, which plays an important role in liver injury repair [89]. Therefore, it is of great significance for further investigation of the mechanism of DILI to simultaneously detect HCIO and H_2S. In 2018, a two-photon and double-response fluorescence probe (probe **44**) was developed for simultaneous discrimination and imaging of HClO and H_2S based on the reaction mechanism of recognition groups which thiolactone and azido were used to recognize HCIO and H_2S, respectively, as well as to act as fluorescence quenchers [90]. Structurally, a fluorophore rhodamine B had a strong fluorescence emission peak at 580 nm when excited at 545 nm, while the other fluorophore 7-amino coumarin emitted a remarkable fluorescence at

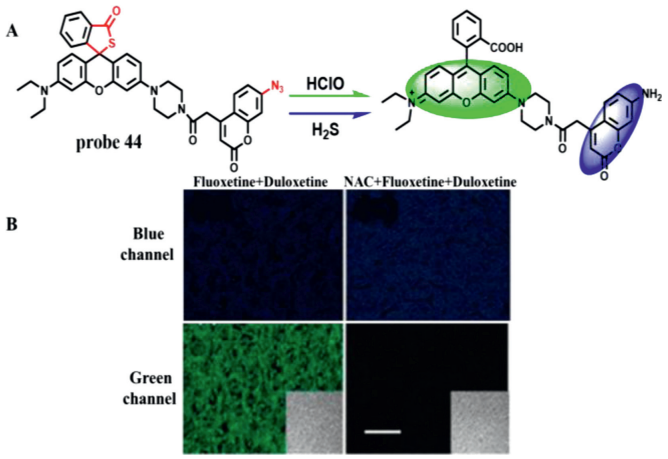

Fig. 33. (A) The reaction mechanism of probe **44** with HClO and H_2S. (B) TPM images of liver slices of mice pre-treated with or without NAC. Copied with permission [90]. Copyright 2018, American Chemical Society.

445 nm after being excited with a wavelength of 360 nm, indicating that the signals of H_2S and HClO did not interfere with each other (Fig. 33A). Probe **44** exhibited excellent selectivity and sensitivity (LOD = 19.8 nmol/L for HClO and 192.1 nmol/L for H_2S). The imaging results in DILI cells and animal models induced by two drugs (fluoxetine and duloxetine) showed that HClO was an appropriate indicator of hepatotoxicity induced by antidepressants, and H_2S played a critical role in the detoxification by supplementing NAC (Fig. 33B).

Epidemiological statistics show that liver injury is an early symptom of inflammation and hepatic failure, manifested by excessive oxidative stress and apoptosis. However, DILI is the most common and unpredictable symptom of liver injury. In 2019, Cheng *et al.* reported a duplex optical probe (probe **45**) which possessed two independent optical channels for sensitive and specific detection of $O_2^{\bullet-}$ and caspase-3 through chemiluminescence (CHL) and NIR fluorescence channels, respectively (Fig. 34A) [91]. With the addition of $O_2^{\bullet-}$, the trifluoromethanesulfonate (TFMS) group on probe **45** was cleaved and a CHL dioxetane was released. The CHL intensity was about 40,000-fold stronger than background and the LOD was as low as about 10 nmol/L. After incubation of probe **45** with caspase-3, the peptide segment (Asp-Glu-Val-Asp) was cleaved and a hemicyanine unit (CyU) was generated at the same time, which resulted in about 12-fold NIRF enhancement at 710 nm. *In vivo* and *in vitro* imaging results not only confirmed the feasibility of probe **45** imaging of $O_2^{\bullet-}$ and caspase-3 in living biological samples (Figs. 34B and C), but also revealed the up-regulation of $O_2^{\bullet-}$ before caspase-3 activation after valproic acid stimulation. However, compared with the high sensitivity of detecting $O_2^{\bullet-}$, the sensitivity of probe **45** to detect caspase-3 is relatively low.

Recently, based on the reaction mechanisms that $O_2^{\bullet-}$ can cleave TFMS, while $ONOO^-$ can oxidize the C=C linker of hemicyanine, Wu *et al.* designed and synthesized a dual-response probe (LW-OTf, probe **46**) for *in situ* imaging of $O_2^{\bullet-}$ and $ONOO^-$ in living cells and mice for the first time (Fig. 35A) [92]. In the presence

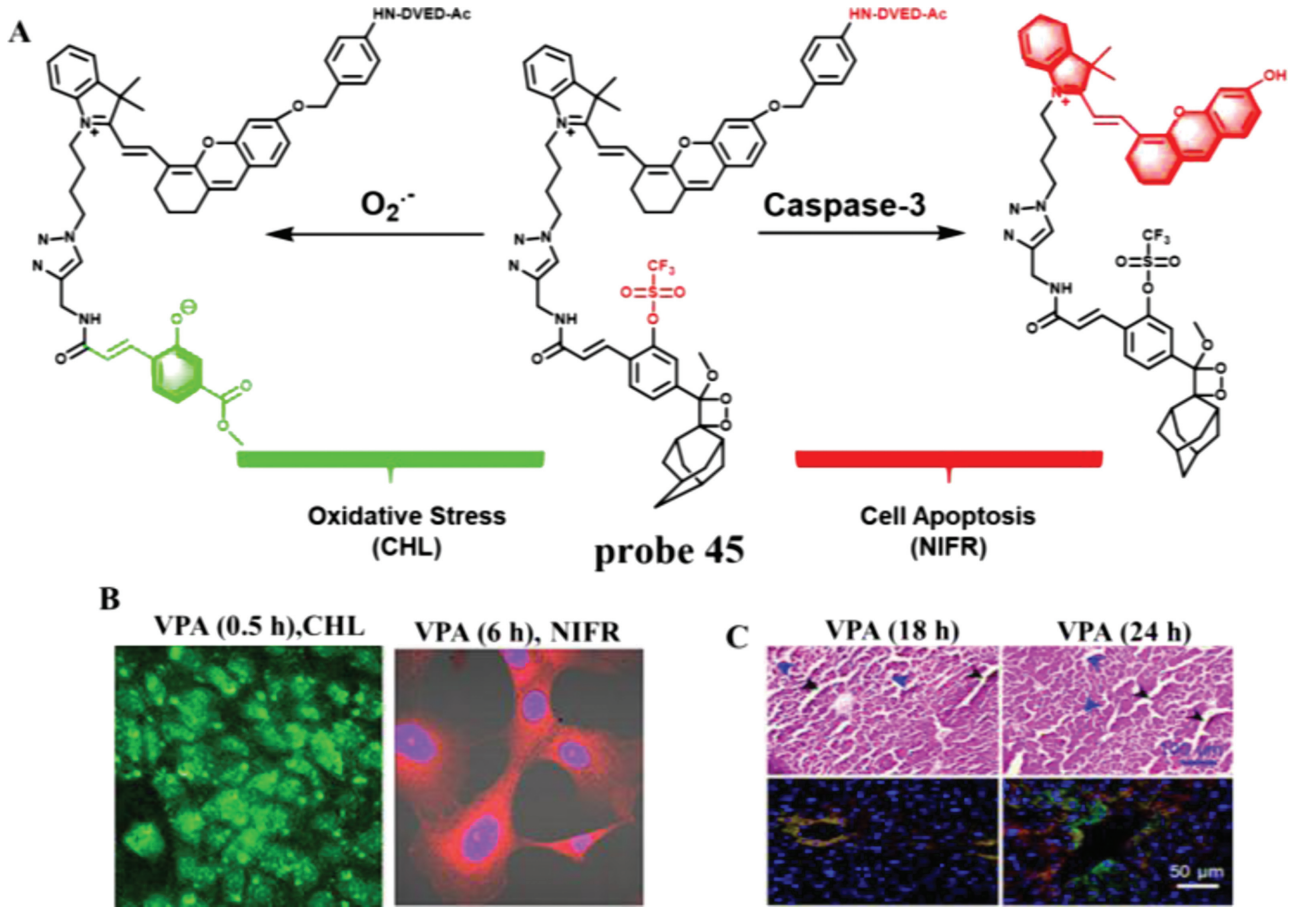

Fig. 34. (A) The reaction mechanism of probe **45** for $O_2^{\bullet-}$ and caspase-3. (B) The duplex imaging of AML-12 cells with VPA before treatment with probe. (C) The H&E staining and immunostaining of mice liver tissues. Copied with permission [91]. Copyright 2019, American Chemical Society.

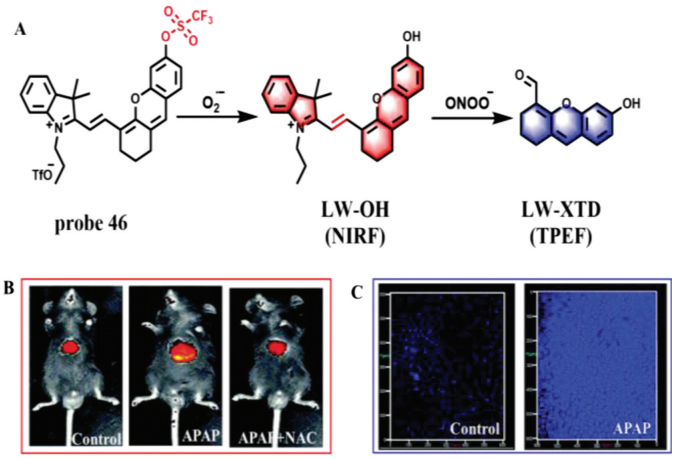

Fig. 35. (A) The reaction mechanism of probe **46** for $O_2^{\bullet-}$ and $ONOO^-$. (B) The NIRF imaging of DILI and remediation. (C) The TP imaging of DILI. Copied with permission [92]. Copyright 2021, Royal Society of Chemistry.

of $O_2^{\bullet-}$, the TFMS group was cleaved from probe **46** to form LW-OH (NIR fluorescence, NIRF) and a 15.6-fold fluorescence enhancement at 710 nm appeared when excited at 675 nm, which resulted in the LOD of 46.5 nmol/L for $O_2^{\bullet-}$. Subsequently, with the addition of $ONOO^-$, the C=C bond was oxidized to form LW-XTD (two-photon fluorescence, TPEF), which exhibited a strong fluorescence intensity at 461 nm at the excitation of 360 nm. The LOD for $ONOO^-$ was calculated to be 38.2 nmol/L. The imaging results of APAP-induced cells showed that probe **46** could monitor the changes of $O_2^{\bullet-}$ and $ONOO^-$ concentration in DILI by NIRF and TPEF, respectively, while both fluorescence channels could be inhibited by *tert*–butylhydroxyanisole (BHA, a ROS and RNS scavenger). The same results were also obtained in APAP-induced mice, which were confirmed by H&E staining of the liver tissues (Figs. 35B and C).

3. Discussion

It has been reported that since the original version of RUCAM was published in 1993, a total of 95,885 cases (from 1993 to June 30, 2020) with liver injury from all over the world, including 81,856 cases of idiosyncratic DILI and 14,029 cases of herb induced liver injury (HILI), have been evaluated by RUCAM [93]. Nowadays, RUCAM is undoubtedly considered as the most widely used method in clinical to assess causality in idiosyncratic DILI and HILI. However, neither the original version nor the updated version of RUCAM is suitable for the assessment of chronic DILI and HILI, and they were also not applicable to the evaluation of suspected DILI and HILI in patients with existing liver disease. In these two cases, the evaluation of DILI often needs more accurate discussion and assessment by the liver disease expert group, especially in the time of onset and the exclusion of other causes of liver injury. Therefore, it is necessary to develop a more efficient and accurate method to diagnose liver injury directly or as an auxiliary RUCAM evaluation.

Generally, DILI is divided into intrinsic DILI and idiosyncratic DILI. Idiosyncratic DILI is a typical human disease, which can hardly be reproducible in animals [94]. Moreover, the mechanism and key biomarkers of idiosyncratic DILI and HILI are still unclear. Although a few fluorescence probes were designed and applied to detect some markers used in RUCAM, such as ALP and GGT, fluorescent probes for the direct diagnosis of idiosyncratic DILI and HILI have not been reported. Intrinsic DILI is mainly caused by the direct toxicity of drugs or their intermediate metabolites to the liver, which is drug dose-dependent and easy to predict in clinical. More importantly, intrinsic DILI can usually be replicated by taking excessive drugs in animals. In the process of taking drugs, a large number of active substances will be released from the liver. By designing fluorescent probes with high sensitivity and specificity to detect these active substances, intrinsic DILI can be assessed or diagnosed. Therefore, compared with idiosyncratic DILI, fluorescent probe technology is more suitable for clinical evaluation and diagnosis of intrinsic DILI. However, unfortunately, because the pharmaceutical and toxicological studies of these reported probes remain largely undisclosed, the evaluation of intrinsic DILI by these probes has been investigated only in cells and animals, but not in DILI/HILI patients. Of course, we believe that with the further unveiling of DILI/HILI formation mechanism and the continuous maturity of fluorescent probe technology, it is very possible to assess DILI (including idiosyncratic DILI and intrinsic DILI) and HILI with safe, efficient and specific fluorescent probe.

4. Conclusion and perspectives

This review summarized the research advances of fluorescent probes for detection of DILI in experimental studies according to various markers of DILI. We believe that these reported fluorescent probes will promote the further development of DILI detection sensors. However, DILI is a very complex disease. Although the reported fluorescent probes can effectively detect the bioactive markers related to DILI, the research on the detection of DILI by fluorescent probes is still in its infancy. For the subsequent development of DILI labeled fluorescent probes, we would like to put forward the following suggestions: (1) at present, most of fluorescent probes for DILI are single indicator imaging, while development of multi-response probes will be an important research direction in the future; (2) it is very necessary to develop newly fluorescent probes with the characteristics of near infrared, good biocompatibility, excellent photostability, high sensitivity and selectivity, fast response and long imaging time; (3) fluorescent probe should be closely combined with clinical diagnosis, preferably integrated with RUCAM method for the evaluation and diagnosis of DILI and HILI; (4) the probes should be able to investigate the mechanism of DILI and its repair, and provide another platform for screening liver protectors or antidotes; (5) specific ligands or related DNA can be introduced into a new probe to make it easy to internalize in hepatocytes and specifically target a certain organelle, which is more conducive to understanding the occurrence and development of DILI; (6) based on the principle of interorgan network interaction, it is necessary to speed up the development of an early warning probe for DILI; (7) in the detection of markers of DILI, more new imaging technologies, such as fluorescence lifetime imaging, super-resolution imaging and 3D photo-acoustic imaging, can be used.

Declaration of competing interest

The authors declare that they have no known competing financial interests or personal relationships that could have appeared to influence the work reported in this paper.

Acknowledgment

This work was supported by National Natural Science Foundation of China (No. U1804136).

References

[1] A. Moles, S. Torres, A. Baulies, C.G. Ruiz, J.C.F. Checa, Front. Pharmacol. 9 (2018) 453.
[2] M. Fung, A. Thornton, K. Mybeck, et al., Ther. Innov. Regul. Sci. 35 (2001) 293–317.

[3] G. Danan, C. Benichou, J. Clin. Epidemiol. 46 (1993) 1323–1330.
[4] C. Benichou, G. Danan, A. Flahault, J. Clin. Epidemiol. 46 (1993) 1331–1336.
[5] G. Danan, R. Teschke, Int. J. Mol. Sci. 17 (2015) 14.
[6] J.E. Teitelbaum, R. Daghistani, Dig. Dis. Sci. 52 (2007) 3396–3398.
[7] R.A. Nathwani, S. Pais, T.B. Reynolds, N. Kaplowitz, Hepatology 41 (2005) 380–382.
[8] V.A. Dixit, L.A. Lal, S.R. Agrawal, WIREs Comput. Mol. Sci. 7 (2017) e1323.
[9] Y. Gao, Y. Lin, T. Liu, et al., Anal. Chem. 89 (2017) 12488–12493.
[10] C. Wen, Z. Zhuang, H. Song, et al., Biomed. Pharmacother. 108 (2018) 208–215.
[11] T. Jiang, P. Rong, W. Wang, Future Med. Chem. 12 (2020) 835–852.
[12] J. Chen, D. Huang, M. She, et al., ACS Sens. 6 (2021) 628–640.
[13] M. Real, M.S. Barnhill, C. Higley, J. Rosenberg, J.H. Lewis, Drug Saf. 42 (2019) 365–387.
[14] F. Wang, K.F. So, J. Xiao, H. Wang, Theranostics 11 (2021) 3317–3330.
[15] G.F. Sueta, R. Radi, ACS Chem. Biol. 4 (2009) 161–177.
[16] N.A. Bonekamp, A. Völkl, H.D. Fahimi, M. Schrader, Biofactors 35 (2009) 346–355.
[17] D. Yang, Y.C. Tang, J. Chen, et al., J. Am. Chem. Soc. 121 (1999) 11976–11983.
[18] D. Cheng, W. Xu, L. Yuan, X. Zhang, Anal. Chem. 89 (2017) 7693–7700.
[19] Y. Li, X. Xie, X. Yang, et al., Chem. Sci. 8 (2017) 4006–4011.
[20] J.B. Li, L. Chen, Q. Wang, et al., Anal. Chem. 90 (2018) 4167–4173.
[21] D. Cheng, J. Peng, Y. Lv, et al., J. Am. Chem. Soc. 141 (2019) 6352–6361.
[22] C. Ling, M. Cui, J. Chen, et al., Talanta 215 (2020) 120934.
[23] M. Schäferling, Angew. Chem. Int. Ed. 51 (2012) 3532–3554.
[24] D. Li, S. Wang, Z. Lei, et al., Anal. Chem. 91 (2019) 4771–4779.
[25] Z. Chen, P. Yan, L. Zou, et al., Adv. Healthc. Mater. 7 (2018) 1800309.
[26] Y. Zhou, P. Li, N. Fan, et al., Chem. Commun. 55 (2019) 6767–6770.
[27] B. Thapa, P. Kumar, H. Zeng, R. Narain, Biomacromolecules 16 (2015) 3008–3020.
[28] A.M. Pujol, M. Cuillel, O. Renaudet, et al., J. Am. Chem. Soc. 133 (2011) 286–296.
[29] C. Liu, Q. Duan, X. Zhang, et al., Sens. Actuators B: Chem. 289 (2019) 124–130.
[30] C. Jin, P. Wu, Y. Yang, Redox Biol. 46 (2021) 102068.
[31] J. Peng, A. Samanta, X. Zeng, et al., Angew. Chem. Int. Ed. 56 (2017) 4165–4169.
[32] Z. Lei, C. Sun, P. Pei, et al., Angew. Chem. Int. Ed. 58 (2019) 8166–8171.
[33] W.L. Jiang, Y. Li, W.X. Wang, et al., Chem. Commun. 55 (2019) 14307–14310.
[34] X. Liu, H. Lai, J. Peng, et al., Small 15 (2019) 1902737.
[35] C. Liu, X. Zhang, Z. Li, et al., J. Agric. Food Chem. 67 (2019) 6407–6413.
[36] G.J. Mao, G.Q. Gao, W.P. Dong, et al., Talanta 221 (2021) 121607.
[37] P. Guerby, O. Tasta, A. Swiader, et al., Redox Biol. 40 (2021) 101861.
[38] Y. Tang, Y. Li, Z. Wang, et al., Chem. Commun. 55 (2018) 27–30.
[39] L. Sun, J. Ouyang, Y. Ma, et al., Adv. Healthc. Mater. 10 (2021) 2100867.
[40] H. Wang, C. Liu, Z. He, et al., Anal. Chem. 93 (2021) 6551–6558.
[41] L. Fang, G. Trigiante, R.C. Otero, et al., Chem. Sci. 10 (2019) 10881–10887.
[42] Y. Zhang, B. Zhang, Z. Li, et al., Org. Biomol. Chem. 17 (2019) 8778–8783.
[43] B. Dong, Y. Lu, N. Zhang, W. Song, W. Lin, Anal. Chem. 91 (2019) 5513–5516.
[44] H. Niu, Y. Zhang, F. Zhao, et al., Chem. Commun. 55 (2019) 9629–9632.
[45] X. Tian, F. Yan, J. Zheng, et al., Anal. Chem. 91 (2019) 15840–15845.
[46] H. Xiao, C. Wu, P. Li, B. Tang, Anal. Chem. 90 (2018) 6081–6088.
[47] G. Nagy, T. Kardon, L. Wunderlich, et al., Arch. Biochem. Biophys. 459 (2007) 273–279.
[48] J.J. Hu, N.K. Wong, S. Ye, et al., J. Am. Chem. Soc. 137 (2015) 6837–6843.
[49] L.L. Zhang, H.K. Zhu, C.C. Zhao, X.F. Gu, Chin. Chem. Lett. 28 (2017) 218–221.
[50] Q. Sun, S.H. Yang, L. Wu, et al., Anal. Chem. 88 (2016) 6084–6091.
[51] Q. Zuo, Q. Wu, Y. Lv, X. Gong, D. Cheng, New J. Chem. 44 (2020) 5457–5462.
[52] D. Roos, Science 296 (2002) 669–671.
[53] M.B. Hampton, A.J. Kettle, C.C. Winterbourn, Blood 92 (1998) 3007–3017.
[54] C. Gorrini, I.S. Harris, T.W. Mak, Nat. Rev. Drug Discovery 12 (2013) 931–947.
[55] J. Yang, X. Zhang, P. Yuan, et al., Proc. Natl. Acad. Sci. U. S. A. 114 (2017) 12384–12389.
[56] D.I. Pattision, M.J. Davies, Curr. Med. Chem. 13 (2006) 3271–3290.
[57] S.T. Manjare, J. Kim, Y. Lee, D.G. Churchill, Org. Lett. 16 (2014) 520–523.
[58] W. Zhang, W. Liu, P. Li, et al., Chem. Commun. 51 (2015) 10150–10153.
[59] G. Li, D. Zhu, Q. Liu, L. Xue, H. Jiang, Org. Lett. 15 (2013) 2002–2005.
[60] W. Chen, W.P. Bay, M.W. Wong, D. Huang, Tetrahedron Lett. 53 (2012) 3843–3846.
[61] X. Xie, T. Wu, X. Wang, et al., Chem. Commun. 54 (2018) 11965–11968.
[62] Y. Deng, S. Feng, Q. Xia, S. Gong, G. Feng, Talanta 215 (2020) 120901.
[63] S.G. Rhee, Science 312 (2006) 1882–1883.
[64] B. D'Autréaux, M.B. Toledano, Nat. Rev. Mol. Cell Biol. 8 (2007) 813–824.
[65] E.A. Veal, A.M. Day, B.A. Morgan, Mol. Cell. 26 (2007) 1–14.
[66] A. Srivastava, J.L. Maggs, D.J. Antoine, et al., Role of Reactive Metabolites in Drug-Induced Hepatotoxicity, in: J. Uetrecht (Ed.), Adverse Drug Reactions, Springer Berlin Heidelberg, Berlin, Heidelberg, 2010, pp. 165–194.
[67] W.L. Jiang, W.X. Wang, J. Liu, Y. Li, C.Y. Li, Sens. Actuators B: Chem. 313 (2020) 128054.
[68] L. Xu, Y. Zhang, L. Zhao, et al., Talanta 233 (2021) 122578.
[69] L. Chen, J. Chen, Y. Fang, F. Zeng, S. Wu, Chem. Commun. 57 (2021) 7842–7845.
[70] Y. Tang, F. Feng, F. He, et al., J. Am. Chem. Soc. 128 (2006) 14972–14976.
[71] C. Liu, W. Chen, Z. Qing, et al., Anal. Chem. 88 (2016) 3998–4003.
[72] B. Ma, M. Lu, B.Y. Yu, J. Tian, RSC Adv. 8 (2018) 22062–22068.
[73] J. Yin, Y. Kwon, D. Kim, et al., J. Am. Chem. Soc. 136 (2014) 5351–5358.
[74] J. Chen, Z. Wang, M. She, et al., ACS Appl. Mater. Interfaces 11 (2019) 32605–32612.
[75] X. Hou, Q. Yu, F. Zeng, J. Ye, S. Wu, J. Mater. Chem. B 3 (2015) 1042–1048.
[76] X. He, L. Li, Y. Fang, et al., Chem. Sci. 8 (2017) 3479–3483.
[77] Y. Huang, Y. Qi, C. Zhan, F. Zeng, S. Wu, Anal. Chem. 91 (2019) 8085–8092.
[78] Y. Yang, L. Zhang, J. Li, et al., Anal. Chim. Acta 1168 (2021) 338621.
[79] G.J. Beckett, G.R. Foster, A.J. Hussey, et al., Clin. Chem. 35 (1989) 2186–2189.
[80] J.D. Hayes, D.J. Pulford, Crit. Rev. Biochem. Mol. Biol. 30 (1995) 445–520.
[81] G.J. Becketta, E.H. Dyson, B.J. Chapman, A.J. Templeton, J.D. Hayes, Clin. Chim. Acta 146 (1985) 11–19.
[82] J. Zhang, Z. Jin, X.X. Hu, et al., Anal. Chem. 89 (2017) 8097–8103.
[83] A. Al Saedi, J. Feehan, S. Phu, G. Duque, Clin. Interv. Aging 14 (2019) 389–398.
[84] P. Zhang, X. Jiang, X. Nie, et al., Biomaterials 80 (2016) 46–56.
[85] X. Tian, F. Yan, J. Zheng, et al., Anal. Chem. 91 (2019) 15840–15845.
[86] D.D. Wang, L.W. Zou, Q. Jin, et al., ACS Sens. 5 (2020) 1987–1995.
[87] T.B. Ren, Z.Y. Wang, Z. Xiang, et al., Angew. Chem. Int. Ed. 60 (2021) 800–805.
[88] Z.M. Prokopowicz, F. Arce, R. Biedron, et al., J. Immunol. 184 (2010) 824–835.
[89] C. Szabó, Nat. Rev. Drug Discovery 6 (2007) 917–935.
[90] X. Jiao, Y. Xiao, Y. Li, et al., Anal. Chem. 90 (2018) 7510–7516.
[91] P. Cheng, Q. Miao, J. Li, et al., J. Am. Chem. Soc. 141 (2019) 10581–10584.
[92] L. Wu, J. Liu, X. Tian, et al., Chem. Sci. 12 (2021) 3921–3928.
[93] R. Teschke, G. Danan, Medicines 7 (2020) 62.
[94] R. Teschke, J. Schulze, A. Eickhoff, G. Danan, Int. J. Mol. Sci. 18 (2017) 803.